Rheology of partially molten plagioclase containing wetting silica-rich anhydrous melt abbreviated title: Rheology of partially molten plagioclase

Alexandre Dimanov

Rheology of partially molten plagioclase containing wetting silica-rich anhydrous melt

abbreviated title: **Rheology of partially molten plagioclase**

Alexandre Dimanov

LMS, UMR7649, Ecole Polytechnique

Route de Saclay, 91128 Palaiseau, France.

Corresponding author: Alexandre Dimanov, *e-mail: dimanov@lms.polytechnique.fr*

Abstract

The present work explores the effects of melt chemistry on diffusion controlled creep of partially molten labradorite plagioclase (An_{50}) at anhydrous conditions. Using sol-gel and hot pressing techniques we produced: 1) nominally melt-free samples (Lab), with < 1 vol. % residual glass confined solely to multiple grain junctions; 2) SilLab1 and SilLab5 partially molten samples containing respectively 1 and 5 vol. % excess amorphous silica, resulting in partial melts wetting numerous grain boundaries as thin (< 10 nm) amorphous films. Energy dispersive X-ray analysis showed that the amorphous phases in Lab, SilLab1 and SilLab5 samples contained about ~ 70, ~ 85 and ~ 95 wt. % $Si0_2$, respectively. Infrared spectroscopy showed that the initial traces of water (~ 0.05 wt. %) were dried out by annealing in air above 1100°C. Uniaxial creep tests performed at 1100 – 1250°C and 3 – 60 MPa flow stresses showed dominantly linear viscous flow, with a strong grain size dependence indicating grain boundary sliding and diffusion control. Counter-intuitively strength and activation energy increased with the content of melts, but in accord with the silica content of the latter, that is with their polymerization state. Our results show that the kinetics of grain boundary diffusion controlled creep strongly depends on melt chemistry. Instead of acting as short–cut for diffusion, thin films of highly viscous amorphous phases may in turn considerably reduce grain boundary transport properties.

Key words: rheology, plagioclase, partial melt, thin melt films, grain sliding, diffusion creep.

1. Introduction

The rheological properties of partially molten silicates may substantially deviate from those of their fully crystalline counterparts. The partially molten silicates are usually substantially weaker (Van der Molen and Paterson, 1979; Vigneresse et al., 1996), but the magnitude of weakening may differ

depending on the minerology and chemistry of the considered system, as well on the proportion of partial melt and its grain scale topology (Cooper and Kohlstedt, 1986; Hirth and Kohlstedt, 1995a; 1995b; Kohlstedt and Zimmerman, 1996; Dimanov et al., 1998; 2000). Understanding the rheological properties of partially molten silicates is therefore of fundamental importance for modelling the dynamics of various tectonic settings. For example, the stability of the high plateau in the collision context of the Himalayan-Tibetan orogen is proposed to be ensured by channel flow localized within the lower crust. The viscosity of the latter is supposedly exceptionally low, in relation with partial melting (see a review by Harris, 2007). Another classical example is the accretion of the oceanic crust from the magma chambers beneath the mid-ocean ridges. In this case, plagioclases and clinopyroxene crystallizing from the basaltic liquid settle down from the crystalline mush at the bottom of the magmatic lens. The gabbroic material is further driven apart from the ridge by the convection of the upper mantle. This lateral flow occurs at partially molten state as demonstrated by the magmatic fabrics: bedding, shape preferred textures and lack of crystalline plasticity (Nicolas and Ildefonse, 1996; Ildefonse and Nicolas, 1997). However, magmatic flow is expected to occur for suspensions at relatively high liquid fractions (> 30 vol. %), which disagrees with the estimations from seismic studies (Lamoureux et al. 1999). Yet, based on microstructural observations Nicolas and Ildefonse (1996) and Lamoureux et al. (1999), suggested that magmatic flow could still operate at low melt fractions (< 10 vol. %) provided flow is accommodated by grain sliding and dissolution – precipitation processes. Such mechanisms have been experimentally observed by Dimanov et al. (1998, 2000) for partially molten plagioclase (labradorite) aggregates presenting melt fractions between 1 – 10 vol. %. The authors emphasized that the topology of the melt was critical with respect to the flow properties. They reported that Newtonian type of flow could be strongly enhanced even for very low melt fractions (1 – 3 vol. %) in the case where the partial melt was wetting most of grain boundaries.

Over more than two decades it was considered that the equilibrium melt distribution in a polycrystalline aggregate is essentially driven by surface tension forces and gradients of chemical

potentials in order to minimise the interfacial free energy (Beere, 1975; Waff and Bulau, 1979, 1982; Bulau et al., 1979; Cooper and Kohlstedt, 1984a; 1984b; 1986; Jurewitz and Watson, 1985; Von Bargen and Waff, 1986; Fujii et al., 1986; Bussod and Christie, 1991; Kohlstedt, 1992; Laporte and Watson, 1995; Laporte et al., 1997; Hirth and Kohlstedt, 1995a,b; Jung and Waff, 1998). From this perspective it can be shown that the equilibrium melt topology at hydrostatic conditions in a partially molten aggregate corresponds to a balance between interfacial tensions at triple points, where two neighbouring solid grains are in contact with the melt. Considering single phase solid matrix, single grain size value, isotropic solid – solid and solid – liquid interfacial energies (γ_{ss} and γ_{sl}, respectively), the latter equilibrium determines an unique dihedral angle θ (the angle between the two solid – liquid interfaces of the two neighbouring grains), which satisfies $2\cos(\theta/2) = \gamma_{ss}/\gamma_{sl}$. In addition, because gradients of chemical potentials of the constituent species appear whenever the system presents solid – liquid interfaces with variable curvatures, the chemical and textural equilibrium requires a constant mean curvature of all the solid – liquid interfaces. In turns, this requirement ensures the minimization of solid – liquid interfacial area and implies concretely that the crystalline phase in contact with the liquid does not present sharp corners and flat surfaces. In summary of the previously cited works, we can consider that at low melt fractions for $\theta > 60°$ the molten phase resides in isolated pockets and interconnectivity occurs only above a critical melt fraction that increases with θ. For $0° > \theta > 60°$ a given fraction of the whole amount of melt, called the equilibrium melt fraction (that minimises the free interfacial energy of the system), forms an interconnected network along three – , four – and higher order grain junctions, whilst all exceeding amount of melt distributes in additional high aspect ratio pools. The smaller is θ and the larger is the proportion of grain boundary area lost to the melt. Grain boundaries are expected to be completely wetted by melt only if $\theta = 0°$. However, since most dihedral angles were found to fall between 10 – 40° in both mafic (olivine or peridotite and basalt, Kohlstedt, 1992) and felsic (granitic rocks and silicic melts, Laporte et al., 1997) systems, two grain boundaries were supposed to be melt-free. But despite the latter expectation, melt films spreading

91 at two grain boundaries were frequently found (Fujii et al., 1986; Bussod and Christie, 1991; Waff and
92 Faul, 1992; Laporte and Watson, 1995; Hirth and Kohlstedt, 1995a,b; Laporte et al., 1997; Faul, 1997;
93 Jung and Waff, 1998; Wark et al., 2003, Carapic et al., 2013). Moreover, instead of the expected smoothly
94 curved solid – liquid interfaces straight flat interfaces (called F – faces) were often observed, suggesting
95 that minimisation of interfacial free energy does not solely relate to minimisation of interfacial area. It
96 was argued that the deviations from the ideal melt topology could relate a) to the polymineralic nature of
97 some of the studied systems, b) to distributed grain sizes and ongoing grain growth, c) to the fact that
98 interfacial free energies and dihedral angles depend on the relative crystal orientations, because silicates
99 present anisotropic surface energies (Waff and Faul, 1992; Laporte and Watson, 1995; Jung and Waff,
100 1998; Cmíral et al, 1998; Schäfer and Foley, 2002, Walte et al., 2003). Theoretical considerations on bi-
101 crystals have shown that interfacial free energies i) are not necessarily much smaller than surface free
102 energies, ii) strongly depend on interfacial misfits, or structural defects (van der Merwe, 2001), and hence
103 on relative grain twist and tilt disorientation.

104 Conversely, non-hydrostatic conditions have also been considered to explain deviations from the
105 ideal melt topology. Melt – wetted grain boundaries were often reported in experimentally deformed
106 partial melts (Van der Molen and Paterson, 1979; Dell'Angelo et al., 1987; Dell'Angelo and Tullis, 1988;
107 Bussod and Christie, 1991; Jin et al., 1994; Hirth and Kohlstedt, 1995a,b; Drury and FitzGerald, 1996;
108 Daines and Kohlstedt, 1997; Zimmerman and Kohlstedt, 1999; De Kloe et al, 2000; Dimanov et al., 2000;
109 Mecklenburgh and Rutter, 2003; Hier-Majumder et al., 2004). This behaviour was attributed to the non-
110 equilibrium dynamic state and/or possibly to undrained conditions at high melt fractions. At high strains
111 major microstructural changes may also occur: melt initially restricted to multiple grain junctions may
112 segregate into high aspect ratio bands preferentially oriented at a small angle ($\approx 20°$) to the direction of
113 maximum compressive stress (Zimmerman and Kohlstedt, 1999; Zimmerman et al., 1999; Holtzman et
114 al., 2003; 2007; Katz et al., 2006; Spiess et al., 2012).

High resolution transmission electron microscopy (HRTEM) studies documented stable thin amorphous films (~ 1 – 10 nm) at grain boundaries in natural xenoliths (Wirth, 1996, Franz and Wirth, 1997), in deformed synthetic olivine – orthopyroxene (Drury and FitzGerald, 1996; De Kloe et al, 2000) and plagioclase (Dimanov et al., 2000) aggregates. Many ceramic materials present the same scheme, with stable nm – sized thin amorphous silica-rich films at grain boundaries (see a review by Willkinson, 1998). It has been demonstrated that such films may be stable, because they tend to decrease the interfacial free energy (Clarke, 1987; Clarke et al. 1993). Conversely, based on HRTEM Hiraga et al. (2002) report that wetting of olivine grains by basaltic melt films is not a general feature. The authors indicate that stable basalt films (~ 10 nm) are only observed along grain boundaries where the grains present low index crystallographic planes.

In the specific case of diffusion-controlled creep of fine grained partially molten rocks with low melt fractions (< 15 vol. %) the strength depends strongly on melt content, but also on the grain – scale melt distribution. Theoretical (Raj, 1982; Pharr and Ashby, 1983; Cooper et al., 1989; Paterson, 2001) and experimental studies on olivine (Cooper and Kohlstedt 1984; 1986; Kohlstedt, 1992; Hirth and Kohlstedt, 1995a, b) and plagioclase (Dimanov et al., 1998; 2000) have shown that strain rates are substantially enhanced if melt films spread along grain boundaries, whilst partial melts that are confined to multiple grain junctions cause only moderate creep rate enhancement. Because diffusion in a molten phase is often orders of magnitude faster than along grain boundaries (see a review in Dimanov et al., 2000), the larger is the proportion of grain boundary lost to the melt, the larger is the proportion of interfaces providing high-diffusivity paths, and the lower is the strength of the partially molten aggregate (Cooper et al., 1989; Paterson, 2001). To date, the effect of melt chemistry on creep rates has essentially been considered from the view point of the dependence of dihedral angles on melt composition (Wanamaker and Kohlstedt, 1991; Kohlstedt, 1992; Wolfenstine and Kohlstedt, 1994). However, for a given melt topology, melt composition might also influence transport properties. In a previous work we

have shown that, at least at the experimental conditions, thin amorphous films were stable in plagioclase aggregates (Dimanov et al., 2000). Most grain boundaries being wetted, the flow strength of the plagioclase aggregates deforming by diffusion controlled grain boundary sliding was substantially depressed, event at very low melt fractions (~ 1 – 2 vol. %). Yet, the activation energy was found to be similar for melt – bearing and nominally melt – free aggregates. Based on extant diffusion data in melts and polycrystalline silicates Dimanov et al. (2000) suggested that in dry conditions the activation energy might be similar for diffusion of network formers along plagioclase grain boundaries and in silica – and aluminium – rich, plagioclase – like melts. In this study we further focus on the effect of the silica content of the wetting intergranular molten phase on grain boundary diffusion controlled creep of partially molten plagioclase aggregates.

2. Experimental procedures

2.1. Specimen preparation

We used fine grained (< 16 μm) labradorite glass powder (Corning Inc., kindly provided by R.C. Cooper). It has $An_{50}Ab_{50}$ chemical composition and X – ray fluorescence (XRF, SRS 303AS) showed that the impurity content was less than 1 wt. % (Tab. 1). After being stored at 120°C in oven for 24 hours the powder was first uniaxially cold – pressed at 300 MPa in steel jackets of 20 mm in length, 10 mm in diameter and 0.5 mm thick. Secondly, the green bodies were hot – isostatically pressed (HIPped) for 3 hours at 1150°C and 300 MPa in a gas-medium Paterson apparatus in order to obtain nearly glass – free polycrystalline material, with about 1 vol. % residual glass (Dimanov et al., 1998; 1999; 2000; 2003; Rybacki and Dresen, 2000). However, this procedure results sometimes in spherulites due to fast crystallization kinetics (Rybacki and Dresen, 2000). Hence, the HIPed samples were re-crushed and

163 milled in alcohol in an agate mortar in order to obtain homogeneously grained crystalline powders. Laser
164 – particle analysis (Fritsch analysette 22) showed that about 80% of the grains were < 10 μm. The larger
165 particles were mostly due to clustering of smaller grains. The chemical composition of the powder was
166 checked by XRF (Table 1). To remove adsorbed water the crystalline powders were annealed at 800°C
167 for 24 hours in air and subsequently stored in an oven at 120°C prior to further processing.
168
169 Table 1. Composition of starting materials and partial melts

Element	An50 glass powder*	An50 crystal powder*	Sol-gel silica*	An50 residual glass**	SilLab5 melt**	SilLab1 melt**
Na_2O(wt.%)	5.68	5.16	0.04	5.5	1.1	2.7
Al_2O_3(wt.%)	28.43	29.07	0.23	29.0	3.3	8.7
SiO_2(wt.%)	55.27	54.82	99.53	53.0	94.8	85.4
CaO(wt.%)	10.52	10.81	0.12	12.0	0.7	2.2
MgO(wt.%)	0.25	0.31	0.06	0.3	0.0	0.0
FeO(wt.%)	0.03	0.04	0.0	0.2	0.2	0.5
Cr_2O_3(wt.ppm)	0.0	0.0	0.0	0.0	0.0	0.3
ZrO_2(wt.ppm)	173	166	0.0	0.0	0.2	0.1
Total(wt.%)	100.2	100.22	98.98	100	100.3	99.9

170 * XRF analysis of powders, **EDX analysis in TEM
171
172 **2.1. a. Melt – "free" samples**
173
174 Crystalline powders were subjected to a second round of cold pressing, followed by HIPing for 24
175 hours at 1150°C and 300 MPa in order to obtain dense, melt – free polycrystalline materials, further
176 referred as Lab samples. Scanning electron microscopy (SEM, Zeiss DSM 962 and Jeol JSM 845) and the
177 line intercept method were applied on carefully polished and thermally etched specimens (Dimanov et al.,
178 1998, 1999, 2000; 2003). Figure 1a shows the obtained microstructures, with lath shaped grains
179 characterized by high aspect ratios and log – normal grain size distribution. We determined a mean
180 arithmetic grain size of 9.8 ± 3.2 μm from five different SEM micrographs. Transmission electron
181 microscopy (TEM, Philips CM 200 Twin) showed that grains present low average dislocation densities
182 and numerous growth twins (Fig. 2a).

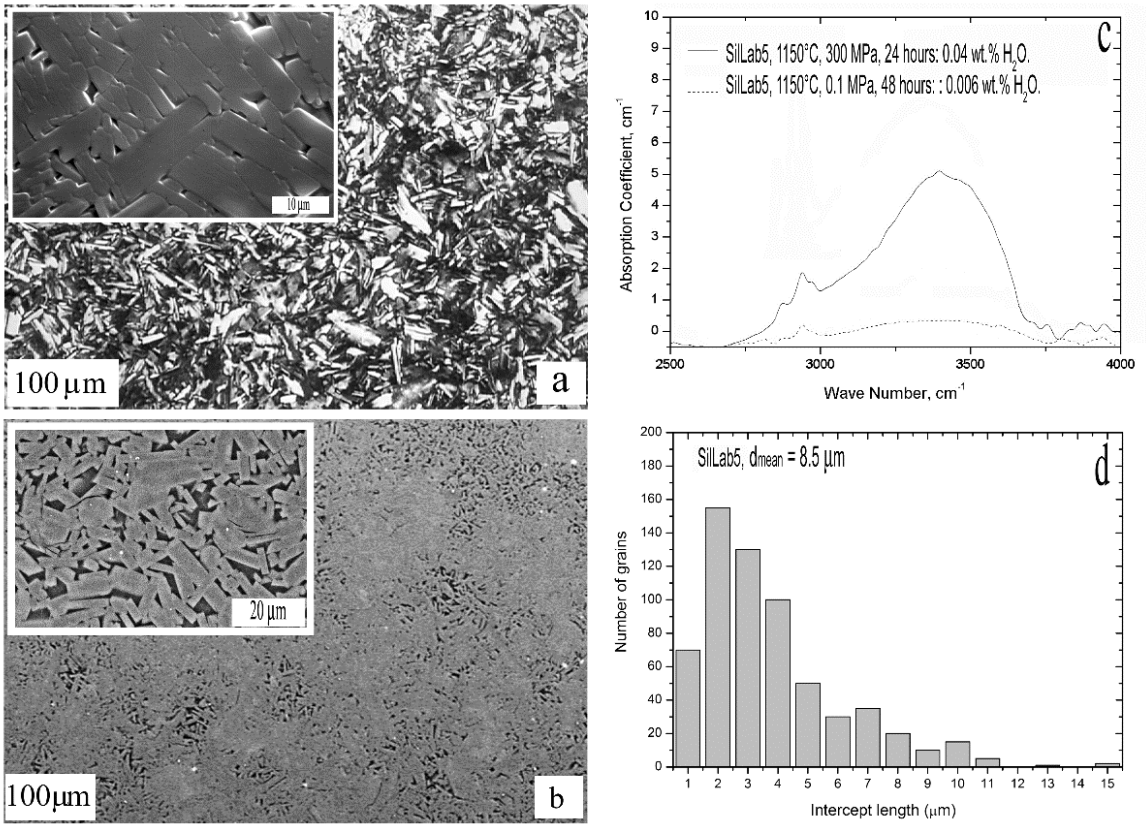

Fig. 1: Characterization of microstructures at optical and SEM scales. a) Optical micrograph of large representative area from thin section and SEM micrograph (insert, SE mode) of polished and thermally etched melt - free specimen (Lab). b) SEM micrographs (BSE mode) of polished melt - bearing specimen (SilLab5). At mm-scale melt distribution is somewhat heterogeneous, with local melt fractions as high as 10 vol. % (insert). c) Water content after initial HIP and after drying anneal from FTIR measurements on SilLab5 samples d) Grain size distribution for SilLab5 samples obtained by the intercept method performed on SEM micrographs.

As previously observed by Dimanov et al., (1998), small amount (< 1 vol. %) of residual glass persisted, but it was essentially restricted to multiple grain junctions (Fig. 2b). Fluid inclusions were also observed within crystals, at grain boundaries and in the glassy-phase. Fourier transform infra-red spectroscopy (FTIR, Brüker IFS 66v) was applied on 5x5 mm^2 doubly polished sections of 150 µm in thickness. We operated in the range 2000 - 4000 cm^{-1} and we applied a third – order polynomial fit for background correction.

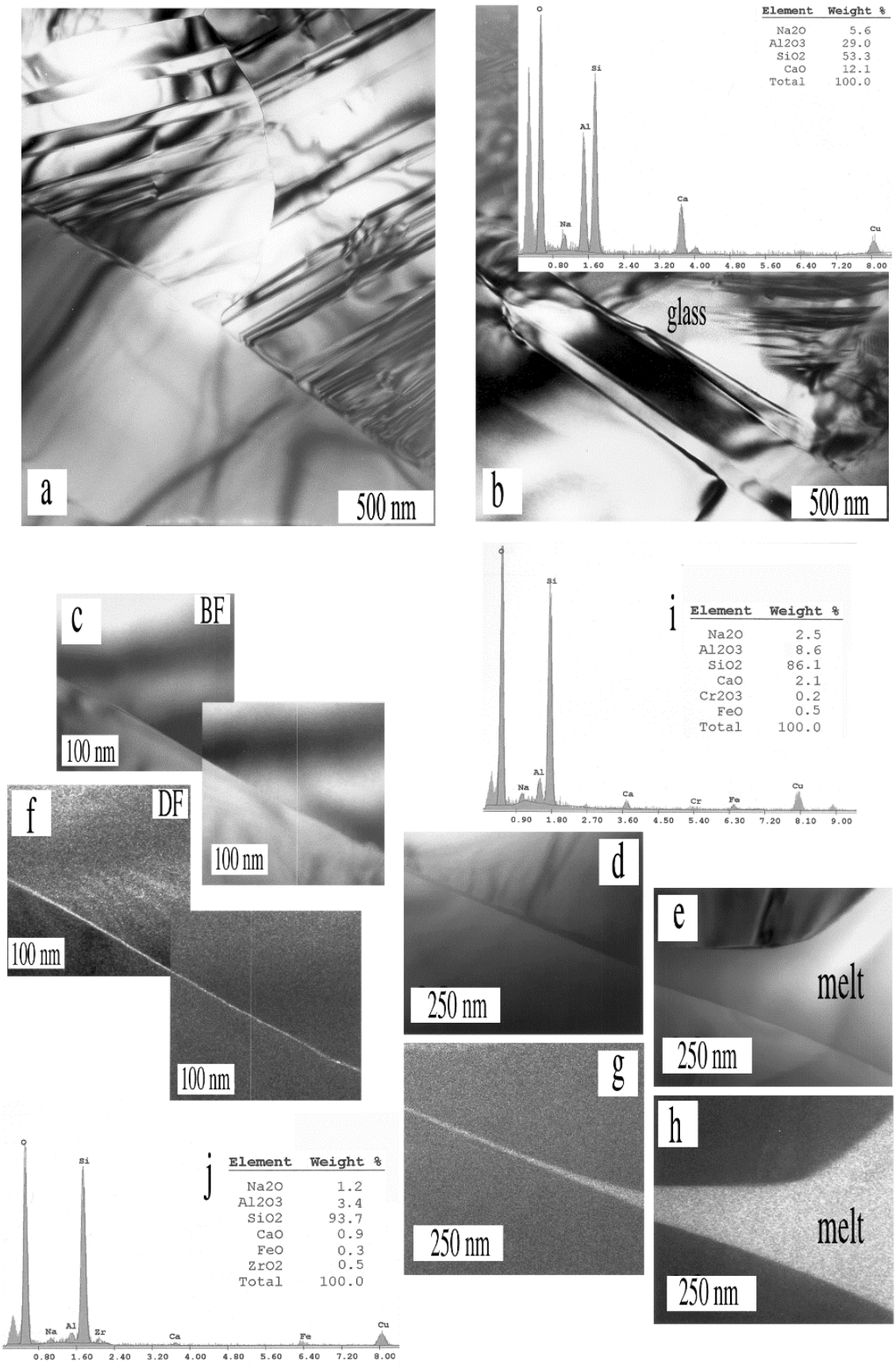
a
500 nm
b
glass
500 nm
Element Weight %
Na2O 5.6
Al2O3 29.0
SiO2 53.3
CaO 12.1
Total 100.0
O
Si
Al
Na
Ca
Cu
0.80 1.60 2.40 3.20 4.00 4.80 5.60 6.40 7.20 8.00
c
BF
100 nm
100 nm
f
DF
100 nm
100 nm
i
Element Weight %
Na2O 2.5
Al2O3 8.6
SiO2 86.1
CaO 2.1
Cr2O3 0.2
FeO 0.5
Total 100.0
O
Si
Al
Na
Ca
Cr
Fe
Cu
0.90 1.80 2.70 3.60 4.50 5.40 6.30 7.20 8.10 9.00
d
250 nm
e
melt
250 nm
g
250 nm
h
melt
250 nm
j
Element Weight %
Na2O 1.2
Al2O3 3.4
SiO2 93.7
CaO 0.9
FeO 0.3
ZrO2 0.5
Total 100.0
O
Si
Na
Al
Zr
Ca
Fe
Cu
0.80 1.60 2.40 3.20 4.00 4.80 5.60 6.40 7.20 8.00

198

Fig. 2: Characterization of microstructures at TEM scale. a) Grains exhibit low dislocation densities, but growth twins are numerous. b) Residual glass pockets (< 1 vol.%) are commonly found at multiple grain junctions in Lab samples. EDX analyses (insert) show that their composition is comparable to plagioclase. c-h) SilLab1 and SilLab5 materials present amorphous pockets at multiple junctions, but most interfaces also show thin amorphous films (< 10 nm) extending from triple junction channels, as evidenced by bright versus dark field imaging. i-j) EDX analysis of amorphous phases performed at melt pockets located at multiple grain junctions in SilLab1 and SilLab5 samples.

As in previous studies (Dimanov et al., 1998; 1999; Rybacki and Dresen, 2000) we observed a broad absorption band centered at about 3350 cm^{-1} (Fig. 1c), indicating free molecular water present in intra – and inter – crystalline fluid inclusions, and/or dissolved within the residual glass and at grain boundaries. But, a few sharper peaks indicated that hydrous species were also incorporated within the crystalline structure (Hofmeister and Rossman, 1985; Beran, 1986; 1987).We calculated the water content of the samples (in mol H_2O/L labradorite), based on Paterson (1982), and using the linear molar absorptivity coefficient for plagioclase (32 L/mol/cm, Beran, 1987). For that purposes, the integral of the spectrum is normalised by the half-width of the absorption band. Assuming a Gaussian approximation, this operation gives the height of the band, which is used together with the linear absorbtivity in the Beer-Lambert's law (see also Dimanov et al., 1998, 1999; Rybacki and Dresen, 2000). The samples contained ≈ 0.05 ± 0.025 wt. % H_2O (≈ 6000 ± 3000 ppm H/Si), which is mostly incorporated by adsorption onto the starting glass particles, and later onto the crystalline particles, during the temporary storage and handling at room condition for cold – pressing. Annealing of the samples for 24 – 48 hours in air at temperatures above 1100°C at 0.1 MPa resulted in drying out most of the water traces down to < 0.002 wt. % H_2O (Fig.1, see also Dimanov et al., 1999).

2.1.b Melt – bearing samples

Dimanov et al. (2000) annealed plagioclase samples (similar to those used in this study) at hypersolidus conditions. The authors obtained partially molten specimens containing a few percent of silica – enriched melt, with up to 80 wt. % SiO_2. In addition to multiple grain junctions the melt was present as thin films (< 5 nm) wetting many grain boundaries. The samples were about an order of magnitude weaker than melt-free specimens. In this study we aimed to investigate the effects of homogeneously distributed and wetting melts with higher silica contents. For this purpose we applied the sol – gel method (Hamilton and Henderson, 1968), which was previously used to precipitate synthetic basalt onto olivine crystalline powders (Cooper and Kohlstedt, 1984; Beeman and Kohlstedt, 1993; Hirth and Kohlstedt, 1995a). We used pure grade tetraethyl orthosilicate ($Si(C_2H_5O)_4$, TEOS from Aldrich) diluted with ethanol in proportions of 10 to 1. Ammonium hydroxide solution (1 mol/l, Prolabo) was used as catalyst. In the solution, water hydrolyzes the TEOS and produces silanol groups (Si-OH), which interact through hydrogen bonding and form hydrolyzed silica. After drying out all volatiles, we performed XRF analysis on the precipitation product that consisted of nearly pure silica (Table 1). We prepared two aqueous solutions, where labradorite powders and diluted TEOS were mixed at the appropriate proportions in order to obtain 1 and 5 vol. % excess silica. The precipitation took place within a few minutes after the addition of the ammonium hydroxide, but the suspensions were continuously stirred for an hour. The precipitation products were dried at 100^{o}C for 24 hours and ground in agate mortar. The resulting powders were fired into platinum crucibles at 700^{o}C (in air) for 24 hours in order to release remaining volatiles. Finally, the silica – coated powders were stored in an oven at 120^{o}C. The coated crystalline powders were cold pressed and HIPed for 24 hours at 1150°C and 300 MPa in order to obtain dense and equilibrated melt – bearing polycrystalline samples for deformation. Samples containing 1 and 5 vol. % excess silica glass are called SilLab1 and SilLab5, respectively. SEM investigations were applied to carefully polished and thermally etched specimens (Fig. 1). The microstructure is comparable to those of melt – free samples, with prismatic and lath shaped grains, and with log – normal grain size distributions

(Fig. 1d). The intercept method determined mean arithmetic grain sizes of 8.6 ± 3.4 and 9.3 ± 3.2 μm for SilLab5 and SilLab1 samples, respectively. The amorphous phases are more or less homogeneously distributed at multiple grain junctions, as evidenced by SEM in back scattering mode (Fig. 1b). TEM consistently showed that the amorphous phases are present at most multiple grain junctions, with variable apparent dihedral angles. Additionally, most two grain boundaries are wetted by thin amorphous layers < 10 nm in thickness. These features are shown in Figures 2c to 2h. In spite of apparently large dihedral angles melt films extend from triple junctions within grain boundaries. In addition, the melt film thicknesses gradually increase in the vicinity of the triple junctions, hence suggesting that there are not finite wetting angles. These observations are in part similar to those of Dimanov et al. (2000) for partially molten plagioclase and of Hiraga et al. (2002) for olivine – basalt system, but we did observe some differences too. In the present study we observed that 1) the melt thickness stabilizes at around 10 nm at distances of less than a micrometer from the triple junction, 2) the melt films are a general feature and not exclusively related to low index crystallographic planes as in the latter study. Energy dispersive X ray analysis (EDX) was performed at triple junctions and evidenced that during HIPing the precipitated silica equilibrated chemically with the residual labradorite glass (≈ 1 vol. %), resulting in liquid phases with ≈ 95 ± 2 wt. % and ≈ 85 ± 2 wt. % $Si0_2$, respectively for SilLab5 and SilLab1 samples (Fig. 2i and 2j, Tab. 1). TEM also evidences the presence of nm scale fluid inclusions in the amorphous phases. FTIR spectroscopy showed similar broad absorption bands and corresponding hydroxyl concentrations (≈ 0.05 ± 0.025 wt. % H_2O) for both melt – bearing and melt – free samples (Fig. 1c). The traces of water could be substantially dried out by annealing in air above 1100°C for 48 hours (Fig. 1c).

2.2. Experimental deformation

Specimens with dimensions of 2.5x2.5x5 mm^3 were cut from hot pressed samples with low speed diamond saw. Compression and observation surfaces were polished to 1 µm and 0.3 µm finish, respectively. Uniaxial creep tests were performed stepwise at constant temperatures and constant loads in a dead-load apparatus (Dimanov et al., 1998; 1999; 2000, 2003). Finite strains for individual steps ranged from 3 to 0.5 %. We used alumina pistons and spacers, with thin platinum foils in order to avoid chemical and to limit frictions. The fixed part of the deformation column was isolated from the outer atmosphere by o – ring tightened alumina tubing, whilst the mobile part benefited from a frictionless oil bath sealing. Dry argon flowed continuously in the furnace tubing. Sample shortening was measured using two linear-variable displacement transducers (LVDT), which inner cores were mounted on two alumina rods ending respectively at the top and bottom spacers. Accordingly, the differential measurements were not affected by temperature fluctuations and allowed for strain rates lower than 10^{-8} s^{-1}. Stress and temperature steps were performed between 3 – 60 MPa and 1100 – 1225°C. Steady state creep rate was generally achieved within less than 0.5 % strain. Total sample strain was less than 15 %. Samples were cooled under load at a rate of 50°/min was in order to preserve at best the in-situ melt topology. However, due to the furnace inertial rapid cooling (within less than 10 mn) was only achieved down to about 900 °C, whilst further cooling down to room temperature lasted for about two hours.

3. Results

3.1. Microstructures

SEM observations did not show any shape preferred orientation of grains in deformed samples. SEM and TEM observations and EDX analysis did not show obvious evolution of melt proportion (within 1 vol. %), topology, or chemistry (within 2 wt. %) during creep. For Lab samples the small amount of

residual glass was never found along grain boundaries. There was no indication for dynamic wetting of grain boundaries during deformation as observed sometimes in olivine-basalt assemblages (Jin et al., 1994; Hier-Majumder et al., 2004). For SilLab1 and SilLab5 samples the initial melt distribution did not obviously change either: most of the melt still resided at multiple grain junctions and the thin melt films were still present at most grain boundaries. Yet, we could evidence some local redistribution of melt along wetted interfaces.

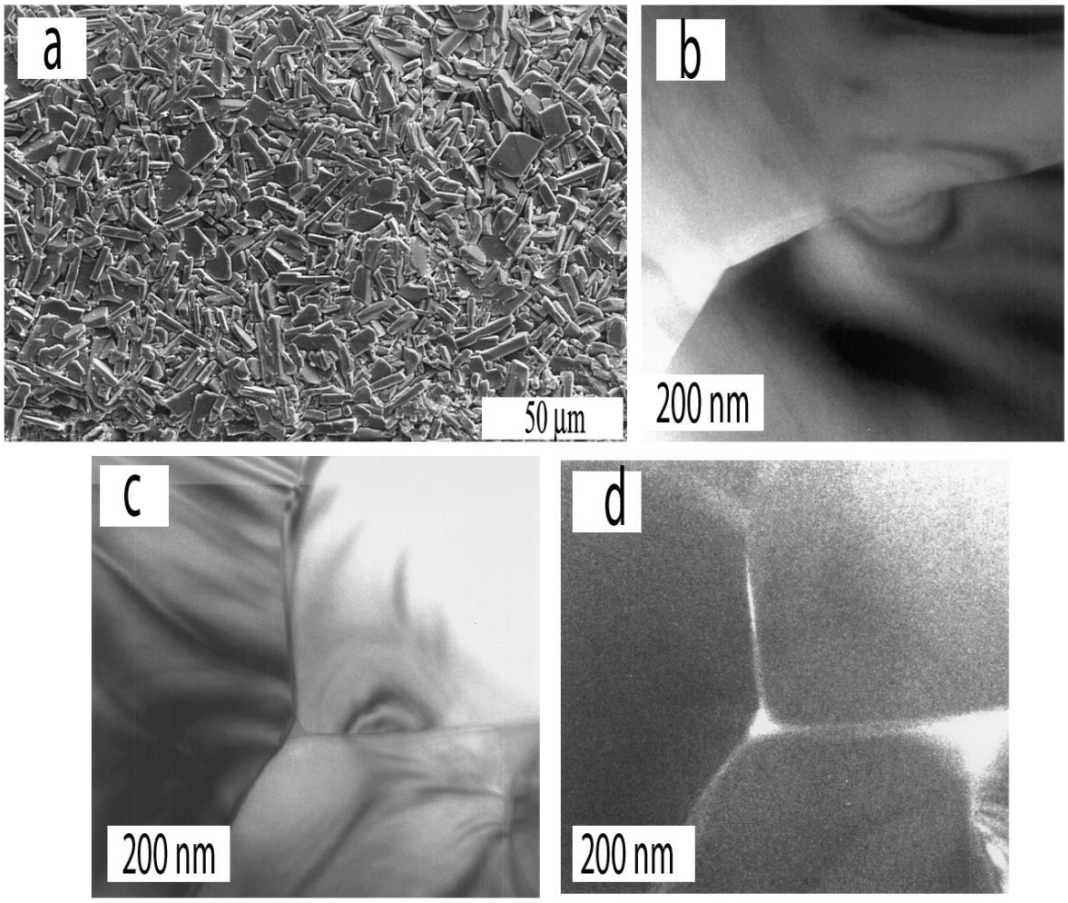

Fig.3: SEM and TEM micrographs of deformed SilLab1 material. a) SEM shows topography development on the sample surface, indicating grain boundary sliding processes. b-c) Bright field images showing dislocation-free grains and whirl shaped strain contrasts next to melt filled pockets (b) or along interfaces (c), which indicate local residual stress related to "dry" contact area (see text). d) Dark field image corresponding to c) showing the presence of amorphous material at interfaces.

Figure 3 shows that along some wetted interfaces the grains present hemispherical strain contrast features. According to Burger et al. (1997), such "strain whirls" result from residual elastic strain, corresponding to local stress enhancement associated with the establishment of local dry contacts along wetted interfaces during creep of glass-ceramic systems. This local phenomenon may be compared with the theoretical island structure proposed by Raj (1982). However, we did not observe massive redistribution of the melt as observed by Jin et al. (1995) in crept glass-ceramic samples or complete melt expulsion out of normally stressed grain boundaries as described for olivine–basalt systems (Jin et al., 1994). Our observations rather support previous authors arguing about the stability of thin amorphous interfacial phases in both static (Clarke, 1987; Hess, 1994) and dynamic conditions (Drury and FitzGerald, 1996).

Curved free dislocations and dislocation arrays could be occasionally observed, but usually dislocation densities, ρ, remained low ($\rho \approx 10^{10} - 10^{11}$ m^{-2}), which is consistent with Newtonian viscous flow operating by grain sliding accommodated by diffusional mass transfer mechanisms. Growth twins are very common in undeformed specimens, hence it is difficult to estimate if mechanical twinning could contribute to deformation. In opposition to polished samples which simply experienced static thermal etching (see Fig. 1), deformed samples present a strong development of surface topography (Fig. 3). Some previous studies on high temperature creep of fine grained zirconia based ceramic materials (Clarisse et al., 2000; Duclos et al., 2002) and superplastic alloys (Huang and Langdon, 2002) report the development of grain scale topography onto the sample free surfaces, which characteristic was interpreted as evidence for grain sliding.

3.2. Mechanical Data

3.2.1. Stress sensitivity

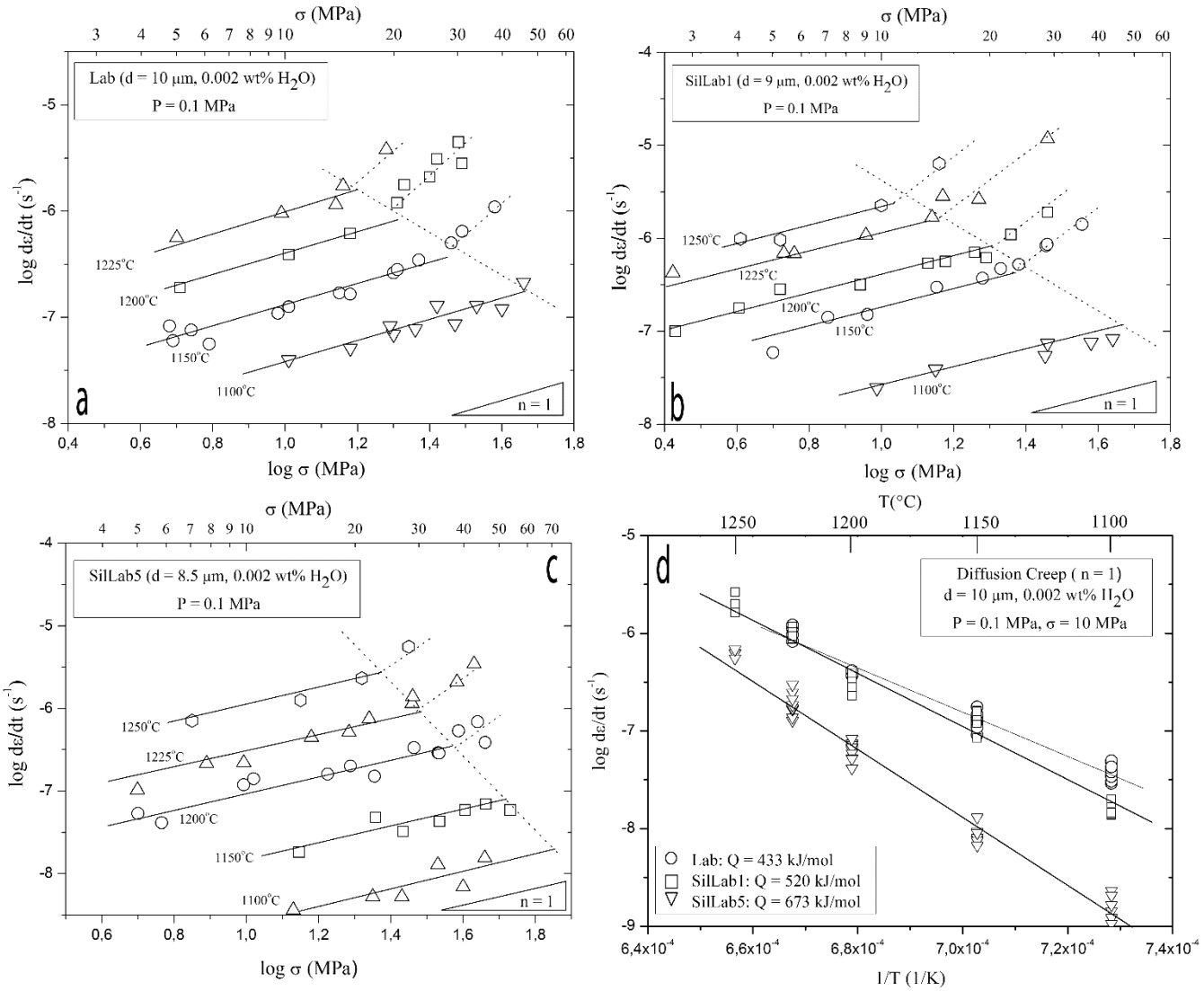

Fig. 4: Thermo-mechanical data for all tested materials presented in log Stress - log Strain rate plots (a, b and c for Lab, SilLab1 and SilLab5 samples respectively) and in Arrhenius diagram (d). All materials show dominantly linear viscous (Newtonian) flow (stress exponent n = 1) and a transition (indicated by dot-line) to non-linear behaviour (dislocation creep) at the highest temperatures and stresses, which is in agreement with previous works on similar materials (Dimanov et al., 1998; 1999; 2000). Data corrected for grain size (see text) and recalculated to 10 MPa differential stress are used to establish the Newtonian flow laws (d). Lab and SilLab materials present comparable strain rates, whilst SilLab5 material is considerably more resistant. Activation energy increases with melt content.

342 Table 2. Mechanical data.

Sample	T(°C)	T(h)	σ_{diff} (MPa)	dε/dt (1/s)
lab-01	1150	31	5.48	7.52×10^{-8}
	1150	13	10.34	1.25×10^{-7}
	1150	8.4	15.25	1.66×10^{-7}
	1150	2.4	20.49	2.82×10^{-7}
	1150	1.5	30.54	6.41×10^{-7}
	1200	0.8	21.34	1.79×10^{-6}
	1200	0.5	26.20	3.06×10^{-6}
	1200	0.5	31.06	2.82×10^{-6}
	1150	25	4.76	8.36×10^{-8}
	1150	3.5	20.01	2.65×10^{-7}
lab-02	1100	17.2	26.19	1.30×10^{-7}
	1100	23	19.43	8.33×10^{-8}
	1100	19.4	22.79	7.75×10^{-8}
	1100	15.2	34.13	1.29×10^{-7}
	1100	8.4	45.36	2.15×10^{-7}
lab-03	1100	66	10.14	4.02×10^{-8}
	1100	21	14.98	5.17×10^{-8}
	1100	24.7	19.82	6.89×10^{-8}
	1100	24	29.73	8.62×10^{-8}
	1100	8.5	39.64	1.21×10^{-7}
	1200	4.8	5.16	1.90×10^{-7}

	1200	1.6	14.98	6.20×10^{-7}
	1200	2.22	10.29	3.88×10^{-7}
	1200	0.97	20.28	1.19×10^{-7}
	1200	0.48	25.12	2.07×10^{-7}
	1200	0.23	29.96	4.43×10^{-7}
lab-05	1150	20	4.92	6.01×10^{-8}
	1150	24.4	9.48	1.10×10^{-7}
	1150	6.4	14.08	1.69×10^{-7}
	1150	2.0	28.61	5.03×10^{-6}
	1150	18	6.17	5.62×10^{-8}
	1150	3.12	23.70	3.50×10^{-7}
	1150	1.13	38.09	1.08×10^{-6}
	1225	2.5	5.01	5.60×10^{-7}
	1225	1.5	9.84	9.53×10^{-7}
	1225	0.72	14.31	1.74×10^{-6}
	1225	0.41	19.18	3.79×10^{-6}
	1225	0.48	13.79	1.14×10^{-6}
SiLab1-01	1150	21	7.11	1.41×10^{-7}
	1150	3.7	14.23	2.98×10^{-7}
	1150	3.23	21.34	4.73×10^{-7}
	1150	1.5	28.59	8.63×10^{-7}
	1150	15	9.15	1.51×10^{-7}
	1150	1.78	28.79	8.33×10^{-7}

	1150	1.83	35.91	$1.44x10^{-6}$
silab1-02	1200	4	4.04	$1.78x10^{-7}$
	1200	16	2.69	$9.97x10^{-8}$
	1200	2.77	8.74	$3.13x10^{-7}$
	1200	1.14	13.45	$5.37x10^{-7}$
	1200	1.15	15.02	$5.60x10^{-7}$
	1200	1.45	18.16	$7.10x10^{-7}$
	1200	1.01	22.87	$1.09x10^{-6}$
silab1-03	1100	30	9.72	$2.45x10^{-8}$
	1100	24.2	14.14	$3.93x10^{-8}$
	1100	14	28.37	$5.47x10^{-8}$
	1100	11.4	13.45	$7.59x10^{-8}$
	1225	2.63	2.65	$4.27x10^{-7}$
	1225	1.33	5.74	$6.85x10^{-7}$
	1225	0.75	9.06	$1.08x10^{-6}$
	1225	1.45	13.79	$1.68x10^{-6}$
	1225	1.01	18.56	$2.62x10^{-6}$
silab1-04	1200	3.1	5.25	$2.82x10^{-7}$
	1200	1.9	19.5	$6.17x10^{-7}$
	1200	1.1	28.84	$1.91x10^{-6}$
	1100	12	28.84	$7.41x10^{-8}$
	1100	10	43.65	$8.32x10^{-8}$
	1150	14.1	5.01	$5.89x10^{-8}$

	1150	2.8	19.06	3.72×10^{-7}
	1150	1.4	23.99	5.25×10^{-7}
	1225	1.2	5.37	6.92×10^{-7}
	1225	0.8	14.79	2.82×10^{-6}
	1225	0.14	28.84	1.18×10^{-5}
	1225	2.4	4.07	9.87×10^{-7}
	1225	2.2	5.25	9.67×10^{-7}
	1225	1.2	10	2.26×10^{-6}
	1225	0.2	14.45	6.37×10^{-6}
silab5-01	1100	22.4	22.63	5.25×10^{-9}
	1100	28.3	34.12	1.28×10^{-8}
	1100	36	46.17	1.54×10^{-8}
	1150	24.2	22.8	4.81×10^{-8}
	1150	20.5	34.31	4.26×10^{-8}
	1150	27	45.99	6.95×10^{-8}
	1200	30.8	5.84	4.16×10^{-8}
	1200	8.2	16.79	1.61×10^{-7}
	1200	4.7	22.63	1.52×10^{-7}
	1200	2.35	33.94	2.91×10^{-7}
	1200	3.2	45.8	3.90×10^{-7}
	1200	7.15	34.12	2.87×10^{-7}
silab5-02	1200	23.2	5.00	5.37×10^{-8}
	1200	17.0	9.84	1.19×10^{-7}

	1200	4.1	19.39	2.01×10^{-7}
	1200	2.55	29.08	3.36×10^{-7}
	1200	2.65	38.62	5.33×10^{-7}
	1200	2.5	43.62	6.11×10^{-7}
	1225	10.2	5.0	1.03×10^{-7}
	1225	3.00	9.84	2.20×10^{-7}
	1225	3.2	19.23	5.16×10^{-7}
	1225	1.0	28.77	1.15×10^{-6}
	1225	0.65	38.32	2.09×10^{-6}
silab5-03	1100	163	13.64	3.63×10^{-9}
	1100	125	26.65	5.26×10^{-9}
	1100	55.8	40.08	6.88×10^{-9}
	1150	61.6	14.01	1.83×10^{-8}
	1150	27	27.15	3.27×10^{-8}
	1150	25	40.29	5.89×10^{-8}
	1150	20.6	53.8	5.83×10^{-8}
silab5-04	1225	19.2	7.83	2.17×10^{-7}
	1225	4.3	14.99	4.47×10^{-7}
	1225	2.5	21.8	7.50×10^{-7}
	1225	1.1	28.84	1.39×10^{-6}
	1225	0.27	42.92	3.46×10^{-6}
silab5-05	1250	3.0	7.01	7.10×10^{-7}
	1250	1.0	14.01	1.60×10^{-6}

	1250	0.5	21.02	2.33×10^{-6}
	1250	0.2	28.25	5.60×10^{-6}

Table 2 reports the experimental data set. Figures 4a, 4b and 4c report the diagrams of log strain rates versus log flow stresses obtained at different temperatures for the different types of materials. All materials showed dominantly a linear relation between strain rates and flow stresses (stress exponent $n \approx 1$), evidencing Newtonian linear viscous flow. Thought, a transition to a power low creep ($n \approx 3$) could be marginally observed at the highest stresses. Depending on temperature and material type the transition stress (σ_t) ranges between $\sigma_t \approx 20 - 60$ MPa. These results are phenomenologically similar to those previously reported for fine grained plagioclase, clinopyroxene and plagioclase-clinopyroxene aggregates (Dimanov et al., 1998; 1999; 2003; Rybacki and Dresen, 2000; Bystricky and Mackwell, 2000; Dimanov and Dresen, 2005; Hier-Majumder et al., 2005), and olivine aggregates (Hirth and Kohlstedt, 1995; Mei and Kohlstedt, 2000; Mei et al., 2002). They indicate two dominant creep mechanisms, which are usually considered as being independent and acting in parallel, with overall dominance of the most effective one. The linear viscous flow that dominates at low stresses is grain size sensitive (gss) and often advocated as being diffusion-controlled creep, whilst the highly non-linear viscous flow that dominates at higher stresses is usually found to be nearly grain size insensitive (gsi) and is attributed to dislocation creep. It has been evidenced that for heterogeneous and/or polyphase materials these mechanisms may be locally concomitant and co-operational (Dimanov et al., 2011), but for homogeneous single phase silicates they are consensually considered as mutually independent. The general flow law resulting from the parallel contribution of both mechanisms is therefore of the form:

$$\frac{d\varepsilon}{dt} = A_{gss}\sigma\, d^{-m} e^{-\frac{Q_{gss}}{RT}} + A_{gsi}\, \sigma^{n}\, e^{-\frac{Q_{gsi}}{RT}} \qquad (1)$$

where $\frac{d\varepsilon}{dt}$ (s^{-1}) is the strain rate, σ (MPa) is the differential stress, n (usually between 3 and 5) is the stress exponent for the dislocation creep component, d (μm) is the grain size, m is the grain size exponent, Q_{gss} and Q_{gsi} (kJ/mol) are the activation energies for the diffusion and the dislocation creep components, respectively. R is the molar gas constant and T is the absolute temperature (K). A_{gss} (s^{-1} MPa μm^m) and A_{gsi} (s^{-1} MPa^{-n}) are material related constants corresponding to the diffusion and the dislocation creep components, respectively. In this study we are essentially interested in the grain size sensitive (Newtonian) regime. Hence, we will further focus only on the data described by the constitutive equation:

$$\frac{d\varepsilon}{dt} = A_0 \sigma e^{-\frac{Q}{RT}} = A \sigma d^{-m} e^{-\frac{Q}{RT}} \qquad (2)$$

where A ($s^{-1}MPa^{-n}\mu m^m$) is the material related constant, that may be written as A_0 ($s^{-1}MPa^{-n}$) if incorporating the microstructural parameter d (μm).

3.2.2. Grain size sensitivity

To estimate the strain rate dependence on grain size for nominally melt – free samples (< 1 vol. % non-wetting residual glass) we considered the present data for Lab samples with a mean grain size of 9.8 μm and data from Dimanov et al. (1998) for similar nominally melt – free labradorite, but coarser grained with a mean grain size of 16 μm. We obtained a grain size exponent m = 2.6 ± 0.3, which is in agreement with previous results for anorthite plagioclase (Wang et al., 1996; Dimanov et al., 1999). Previous studies on olivine and olivine – basalt systems (Hirth and Kohlstedt, 1995) documented similar grain size sensitivities (m ≈ 2.5 – 3) indicating grain boundary diffusion controlled creep (Coble, 1963). Dimanov et al. (2003, 2007) also reported similar grain size exponents for fine grained diopside samples, and Dimanov et al., (2007) documented microstructural evidences for grain sliding mechanisms accommodated by diffusional mass transfer in fine grained anorthite and diopside two – phase aggregates.

386 According to Coble (1963) and Ashby and Verall (1973), the present data indicate that grain sliding
387 accommodated by grain boundary diffusion most likely operated in the linear – viscous regime.
388
389 **3.2.3. Activation energy**
390 In Figure 4d we reported the flow laws for the different materials in an Arrhenius type of diagram,
391 where log strain rates (for a fixed grain size and flow stress) are plotted as a function of the inverse absolute
392 temperature. The slopes of the linear regressions provide the activation energies Q = 433 ± 14 kJ/mol, Q
393 = 520 ± 21 kJ/mol and Q = 673 ± 18 kJ/mol for diffusion controlled creep of dry Lab, SilLab1 and SilLab5
394 samples, respectively (Tab. 3). The activation energy and the strain rates for our Lab samples are
395 comparable with those for diffusion controlled creep of labradorite (An60) and anorthite plagioclase
396 aggregates, deformed uniaxially at 0.1 MPa (Dimanov et al., 1998, 1999). Figure 4d also shows that i) the
397 strain rates are nearly identical for Lab and SilLab1, ii) SilLab5 samples (which contain the highest
398 proportion of melt) show substantially lower strain rates, iii) the activation energy increases with the
399 addition of silica – rich melt.
400
401 **3.2.4 Melt effects**
402 Mechanical characterization (stress exponent, grain size exponent) and microstructures indicate
403 that all kind of samples deformed dominantly by grain sliding mechanisms accommodated by grain
404 boundary diffusion. These results agree with previous studies on high temperature creep of partially
405 molten labradorite An60 containing either non – wetting residual An60 glass (Dimanov et al., 1998), or
406 wetting partial melt obtained at sub solidus conditions (Dimanov et al., 2000). For instance, Dimanov et
407 al. (2000) have shown that samples containing ≈ 2 - 3 vol. % of wetting partial melt (thin melt films
408 present at numerous grain boundaries) were substantially weaker than melt – free samples, or than samples
409 containing similar amounts of non – wetting residual glass (present only at multiple grain junctions).

Conversely, in the present study we clearly observed that the presence of thin amorphous films at grain boundaries did not weaken the samples. SilLab1 samples exhibited comparable strain rates and activation energy as for melt – free Lab samples, whilst counter intuitively SilLab5 showed to be substantially stronger and to have much higher activation energy than any other tested samples. The present results indicate that the mechanical behaviour of the partially molten samples does not only depend on the melt proportion and distribution, but also on the melt chemistry and more specifically on the silica content of the amorphous phase: the higher was the silica content and the lower was the creep rate, and hence the diffusion kinetics controlling mass transfer.

3.2.5 Flow laws

The flow law parameters that we obtained by least square regression fits of equation (2) to the mechanical data of the Newtonian regime for Lab, SilLab1 and SilLab5 materials are listed respectively below for a grain size d = 10 μm (assuming m = 3):

For Lab : $\log A_0\ (s^{-1}MPa^{-n}) = 9.026 \pm 0.524$, $n = 1$, $Q = 432.889 \pm 14.234$ kJ/mol

For SilLab1 : $\log A_0\ (s^{-1}MPa^{-n}) = 12.079 \pm 0.757$, $n = 1$, $Q = 520.484 \pm 21.000$ kJ/mol

For SilLab5 : $\log A_0\ (s^{-1}MPa^{-n}) = 16.732 \pm 0.642$, $n = 1$, $Q = 673.342 \pm 17.864$ kJ/mol

4. Discussion

To our knowledge, the only previous work concerned with high temperature creep of silicate polycrystalline material containing excess pure silica is from Wolfenstine and Kohlstedt (1994). In the latter study synthetic Nickel – based olivine aggregates containing 3 % pure silica in excess have been deformed in uniaxial compression. The presence of the amorphous silica did not affect the creep properties

of the samples. Marked weakening was observed only at temperatures promoting kinetic decomposition of the Ni – olivine. However, the material preparation procedure was different. Also, the authors observed that the excess silica was exclusively restricted to multiple grain junctions, whilst two grain boundaries remained melt-free. It is therefore impossible to directly compare the results of Wolfenstine and Kohlstedt (1994) and the present findings. Conversely, our present data may be compared with the results of previous works of Dimanov et al. (1998; 2000). These former studies have clearly documented that for partially molten plagioclases samples containing plagioclase – like partial melts (with silica content < 80 wt. %), and deforming by diffusion controlled grain sliding, the creep strength depends mostly on the melt topology. Dimanov et al. (2000) concluded that the samples exhibiting amorphous films along most grain boundaries are substantially weaker than samples presenting an interconnected amorphous network along multiple grain junctions but crystalline grain boundaries. The present study further shows that for diffusion controlled grain sliding at dry conditions (< 0.002 wt.% water), when the physical structure of grain boundaries is amorphous (presence of thin melt films), the chemistry of the amorphous phase (and more specifically the silica content) is the key criterion for the creep strength. On the one hand, materials which are nominally fully crystalline and materials containing ≈ 2 vol. % of wetting partial melt with ≈ 85 wt. % silica have similar creep strengths. In opposition, samples with ≈ 6 vol. % wetting partial melt, but containing ≈ 95 wt. % silica present pronounced strengthening. Though astonishing, this situation is not unique. Numerous studies show that silicon nitride and silicon carbide ceramics almost always present ≈ 1 – 2 nm amorphous silica films along most grain boundaries. Still, these materials present exceptional creep strengths at high temperatures (see a review of Meléndez-Martinez and Dominguez-Rodriguez, 2004 and references therein). Kajihara et al. (1995) have shown that between 1200 – 1380°C tetragonal zirconia polycrystals with amorphous silica present at grain boundaries is characterized by superplasticity involving grain boundary sliding and diffusion controlled viscous flow of the silica phase, with an activation energy of 635 kJ/mol. Ojovan and Lee (2004) reported that enthalpies of formation and

458 migration of defects in pure silica are respectively of 197 and 515 kJ/mol, which summation is in
459 astonishing agreement with both the latter activation energy and the value we report for creep in SilLab5
460 samples (673 kJ/mol), where the controlling mechanisms is supposedly grain boundary diffusion through
461 extremely silica-rich melt films. Considering that we observe diffusion controlled creep and clear effects
462 of the melt chemistry it is useful to estimate the viscosities and the diffusion properties of the melts present
463 in our samples in order to provide a physical – chemical explanation of the creep strength of our materials.
464
465 **4.1. Viscosities of the silicate melts**
466
467 The estimation of the viscosities of natural silicate melts is a crucial issue in earth sciences.
468 Therefore, their dependence on temperature and composition has been extensively studied experimentally
469 and theoretically (see Giordano et al. 2006, 2008 and references therein). From a general view point the
470 viscosity of a melt essentially depends on the degree of polymerisation of its structural units (Mysen,
471 1983). The latter is often expressed in terms of the NBO/T number, which is the number of non-bridging
472 oxygen per tetrahedron. Species in tetrahedral coordination (in particular Si^{4+} and Al^{3+}, but also Ti^{4+}, Fe^{3+}
473 ...) tend to polymerize the melt by establishing a tri-dimensional network of tetrahedrons and are thus
474 called network formers, whilst metal, alkaline and earth alkaline cations have the opposite tendency and
475 are therefore called network destroyers. The NBO/T directly relates to the relative amounts of network
476 formers and network destroyers. The lower is the NBO/T the more viscous is the considered melt. For
477 example, basalts are characterized by NBO/T ranging between 1 – 2 and are many orders of magnitude
478 less viscous than granitic and plagioclase like melts, not even mentioning fully polymerized amorphous
479 silica, which is characterized by NBO/T = 0. Based on numerous experimental data sets Giordano and
480 Dingwell (2003), and more recently Giordano et al. (2006, 2008), proposed semi empirical models for
481 predicting viscosities of anhydrous and hydrous silicate melts over a wide compositional range (from

haplogranitic to basaltic compositions). Data sets were first described with the well-known Vogel-Flucher-Tammann empirical relation:

$$\log\eta = A + \frac{B}{T - C} \qquad (3)$$

where η is the viscosity (in Pa s), T is the absolute temperature (in K), A, B and C are the fitting parameters. The analysis is further constrained by the hypothetical assumption that the viscosities of all silicate melts converge to a common value at extremely high temperatures. This analysis implies that: i) A is composition independent, ii) B and C are correlated and accommodate all compositional effects. In particular, B and C correlate with the polymerization degree and the composition. The authors express the latter by the SM (structure modifier) parameter, which is (for anhydrous melt) the sum of the molar proportions of alkalis and earth alkaline network modifiers (SM = Σ mol.% = Na_2O + K_2O + CaO + MgO + MnO + FeO_{Tot}/2). Based on (3) Giordano et al. (2006) computed the isothermal viscosities for 44 different melt compositions (44 different SM) corresponding to different peraluminous, metaluminous and peralkaline silicate melts. The obtained isothermal viscosity values were further fitted to empirical equations of the form:

$$\log\eta = a_1 + \frac{a_2 a_3}{a_3 + SM} \qquad (4)$$

where a_i, (i = 1, 2, 3) are empirical (temperature dependent) fitting parameters. According to the adjustments of the model to the experimental data for 44 different melts the authors derived a_1, a_2, a_3 as functions of temperature between 700°C and 2000°C (Tab. 4, Giordano et al., 2006).

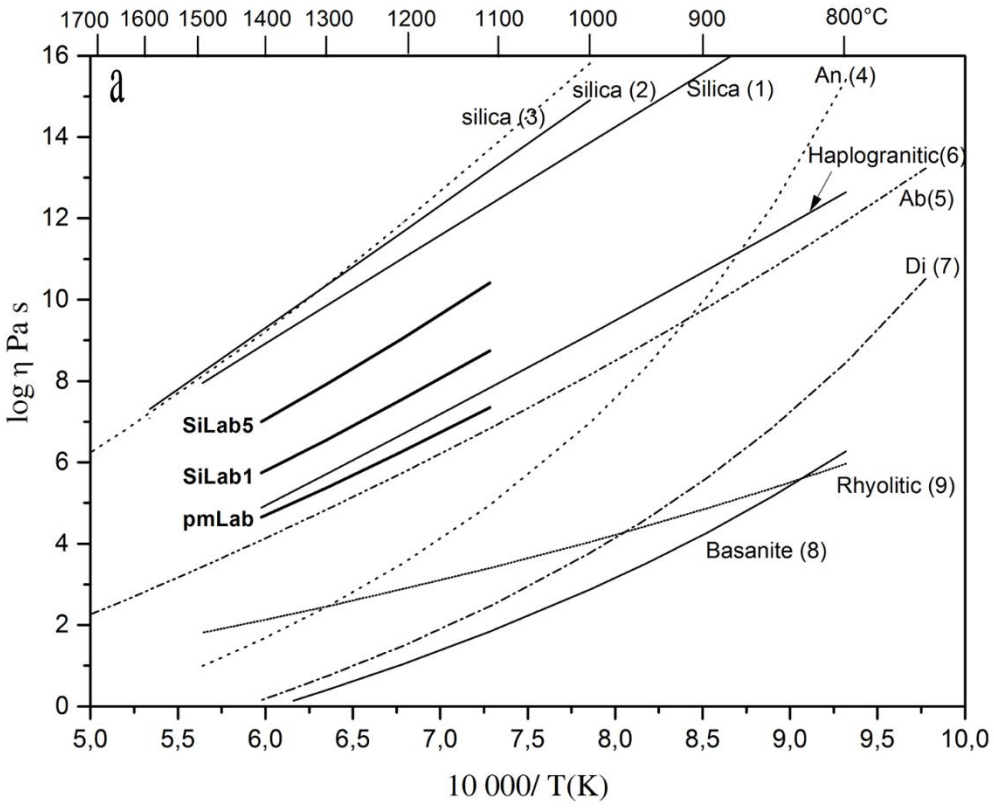
1700 1600 1500 1400 1300 1200 1100 1000 900 800°C
a
silica (3)
silica (2)
Silica (1)
An.(4)
Haplogranitic(6)
Ab(5)
Di (7)
SiLab5
SiLab1
pmLab
Rhyolitic (9)
Basanite (8)
log η Pa s
10 000/ T(K)

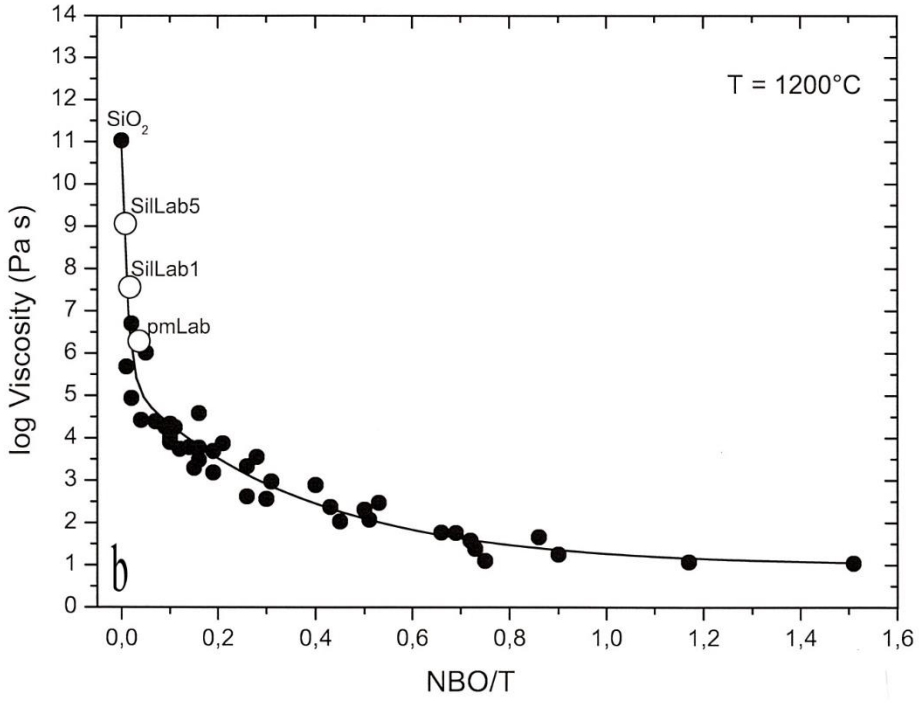
T = 1200°C
SiO2
SilLab5
SilLab1
pmLab
b
log Viscosity (Pa s)
NBO/T

504

Fig. 5: Comparison between calculated or measured viscosities of typical silicate melts and viscosities calculated for the melt compositions of those present in our materials. a) Arrhenius plot of viscosities of typical silicate melts (not exhaustive, but covering the whole range of viscosities from basaltic composition to vitreous silica) and those of the melts present in our samples (SilLab1 and SilLab5) and in the partially molten samples (pmLab) of Dimanov et al. (2000), computed with the model of Giordano et al. (2008). Data for silica are: (1) from Giordano et al., (2005), (2): from Nascimento and Zanotto, (2006), Silica (3): from Ojovan and Lee (2004) and from experimental data of Urbain et al., 1982 and Hetherington et al (1964). Anorthite (An(4)) and Diopside (Di(7)): from Russel and Giordano (2005), Haplogranitic(6), Albite (Ab(5)) and Rhyolitic(9): from Giordano et al. (2005), Basanite(8): from Giordano et al. (2006). b) Comparison of the experimental viscosities used by Giordano et al. (2008) to set the parameters of their model and the viscosities computed with the latter for compositions of melts as those present in our materials as a function of the NBO/T number. The model predicts very well the viscosities of the melts present in our samples.

The phenomenological model of Giordano et al. (2006) was initially derived on the basis of experimental results from silicate melts which silica content did not exceed 80 wt. % (rhyolitic melt), but according to Giordano et al. (2008) the model may be applicable for melts containing up to 90 wt. % silica, which is the case for the melt present in our SilLab1 materials (≈ 85 wt. % SiO_2, SM = 5.15). Due to the lack of any alternative model, and as a first order approximation, we also used the equation (4) and the a_i parameters given by Giordano et al. (2006) in order to calculate the viscosity for the melt present in our SilLab5 (≈ 95 wt. % SiO_2, SM = 2.56) samples. The viscosity results are plotted as functions of the inverse absolute temperature in Figure 5a. One can see that the melt present in SilLab5 samples (our silica – richest melt) is about one to two orders of magnitude more viscous than the melt present in SilLab1 samples. We have also reported for comparison (i) the computed viscosities for diverse anhydrous silicate melts (haplogranitic, plagioclases, rhyolitic, diopside and basanite) calculated by Russel and Giordano (2005) and Giordano et al. (2006) on the basis of equation (4), (ii) some experimentally derived viscosities for silica, albite and basalt melt (see references in figure caption). The data in Figure 5a show that silica is the most possibly viscous melt, whilst mafic and ryolitic melts are the less viscous ones. Plagioclase

and haplogranitic melts present intermediate viscosities. The viscosities we obtain for the melts present in our samples are in between those for pure silica and haplogranitic/albitic melts, which is fully consistent with the fact that their silica contents are extremely high. We also considered for comparison the composition data for the silica – rich (≈ 80 wt. % SiO_2, SM = 8.39) partial melt present in the partially molten labradorite (called pmLab) from Dimanov et al. (2000). The corresponding viscosity is substantially lower (one to three orders of magnitude) than those of the melts investigated in the present study, and compares well with the viscosities for haplogranitic or albitic melts.

We also calculated the NBO/T for the melts in the present study and the study of Dimanov et al. (2000) following the approach of Mysen (1983, 1988; 2003). As a first order approximation we considered only the major cations present (Si, Al, Na, Ca). In particular, all Al present was assigned to tetrahedral coordination (network former), as its content does not exceed the sum of the charge weighted contents of Na and Ca (Al < Na + 2Ca). We obtained NBO/T values ≈ 0.01, 0.02 and 0.06 for SilLab5, SilLab1 and pmLab respectively, which clearly indicate polymerization states in agreement with the calculated viscosities. In addition, we realized a comparison of the viscosities of the melts present in our samples and the material from Dimanov et al. (2000) and the viscosities of all the different melts reported by Giordano et al. (2006) against their NBO/T numbers, at 1200°C (Fig. 5b). The data set is fully consistent, including for the silica-richest melt from our SilLab5 material. The calculated viscosities of the melts from SilLab5, SilLab1 and pmLab materials correlate very well with the viscosity suite for all the melts considered by Giordano et al. (2006), which suggests that the extrapolation we made in using their model for the silica-richest melt from SilLab5 sample is reasonable.

4.2. Melt diffusivities versus grain boundary diffusivities

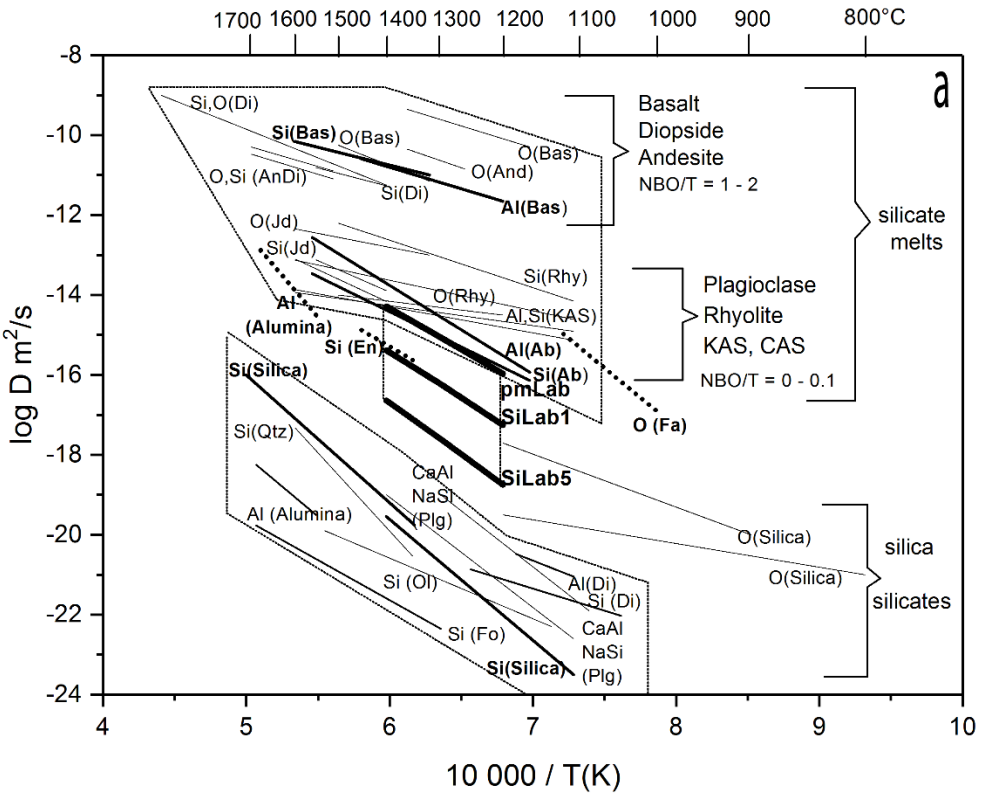
1700 1600 1500 1400 1300 1200 1100 1000 900 800°C
a
log D m²/s
10 000 / T(K)
Si,O(Di)
Si(Bas)
O(Bas)
O(Bas)
O(And)
O,Si (AnDi)
Si(Di)
Al(Bas)
O(Jd)
Si(Jd)
Si(Rhy)
O(Rhy)
Al
(Alumina)
Al,Si(KAS)
Si (En)
Al(Ab)
Si(Ab)
Si(Silica)
pmLab
SiLab1
O (Fa)
Si(Qtz)
SiLab5
CaAl
NaSi
(Plg)
Al (Alumina)
O(Silica)
O(Silica)
Si (Ol)
Al(Di)
Si (Di)
CaAl
NaSi
(Plg)
Si (Fo)
Si(Silica)
Basalt
Diopside
Andesite
NBO/T = 1 - 2
Plagioclase
Rhyolite
KAS, CAS
NBO/T = 0 - 0.1
silicate
melts
silica
silicates

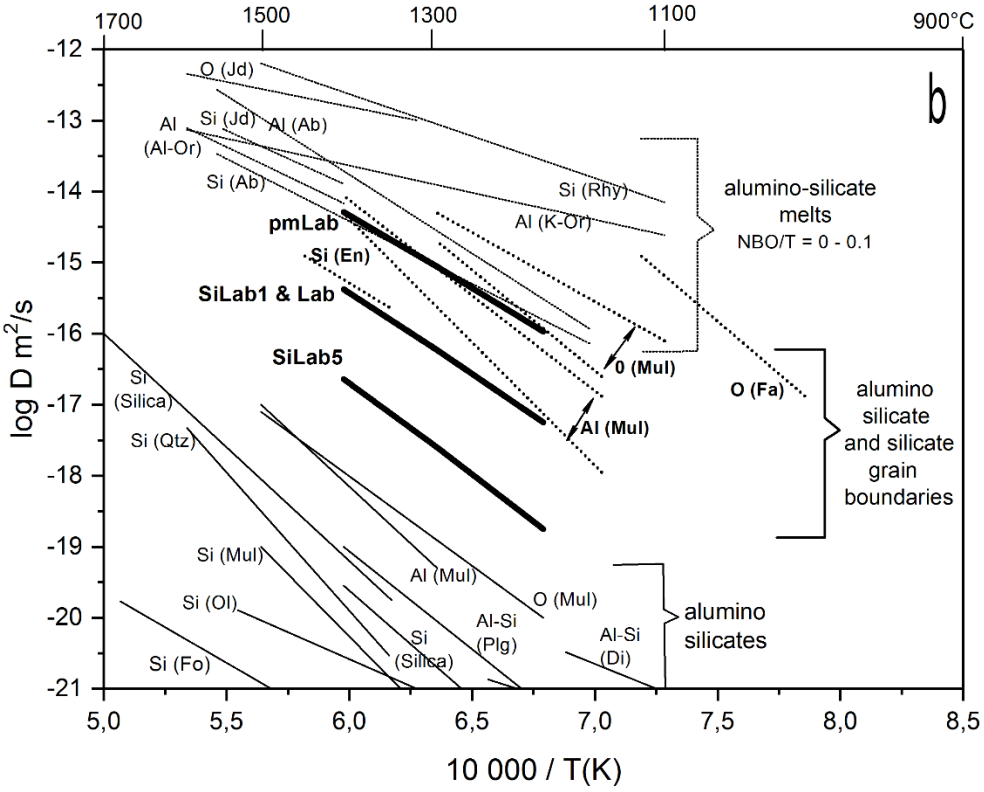
1700 1500 1300 1100 900°C
b
log D m²/s
10 000 / T(K)
O (Jd)
Al
(Al-Or)
Si (Jd)
Al (Ab)
Si (Ab)
Si (Rhy)
Al (K-Or)
pmLab
Si (En)
SiLab1 & Lab
SiLab5
O (Mul)
O (Fa)
Al (Mul)
Si
(Silica)
Si (Qtz)
Si (Mul)
Al (Mul)
O (Mul)
Si (Ol)
Al-Si
(Plg)
Al-Si
(Di)
Si
(Silica)
Si (Fo)
alumino-silicate
melts
NBO/T = 0 - 0.1
alumino
silicate
and silicate
grain
boundaries
alumino
silicates

553

Fig. 6: Arrhenius diagram of volume and grain boundary diffusion of network formers (Si, Al and O) in silicates and oxides and in silicate melts (in dry or unsaturated conditions). **a:** The dot line delimited upper and lower fields represent the data for Si, Al and O diffusion in silicate melts and silicate single crystals, respectively. The data are recalculated for a pressure of 0.1 MPa (when activation volumes were available). Bas is basalt, Rhy is rhyolitic melt, Di and Jd refer to diopside and jadeite melts, Ab and KAS are albite and potassium-aluminosilicate melts. Diffusivity of Si in silica falls within the lower field for volume diffusion. Diffusivities of O in silica fall in-between the two fields. Grain boundary diffusivities (recalculated for a grain boundary width of ~ 3 nm) are represented by heavy dot lines. The larger vertical brackets indicate the type of diffusivity. For diffusion in melt the smaller brackets indicate the compositional ranges and the corresponding NBOT numbers. The diffusivities calculated for our melt compositions (see text and Fig. 5) are reported as heavy lines

b: Close up from (a) comparing the existing grain boundary diffusivities (light doted lines) in aluminosilicates and silicates (Mulite: Mul, Enstatite: En, Fayalite: Fa) and calculated diffusivities for the present highly polymerized aluminosilicate melts (pmLab, SilLab1 and SilLab5). It appears that grain boundary diffusivities are in general comparable to the lowest diffusivities in alumino-silicate melts, as do the diffusivities for pmLab and SilLab1 melts. The diffusivity for SilLab5 melt shows however substantially lower, in-between the lowest diffusivities in alumina-silicate melts and the highest diffusivities in alumina-silicate single crystals.

Diffusion data for melts are from Baker (1990, 1992, 1995), Shimizu and Kushiro (1984, 1991), Canil and Muehlenbach (1990), Wendlandt (1991), Chakraborty et al. (1995), Kress and Ghiorso (1995), Lesher et al. (1996), Harmer and Brook (1980), Brebec et al. (1980), Reid et al. (2001).

Data for grain boundary diffusion in silicates, aluminosilicates and alumina are from Rubie (1986), Fisler and Mackwell (1994), Fisler et al. (1997), Fielitz et al. (2004, 2007, 2016). Data for volume diffusion in silicates, aluminosilicates and alumina are from Bejina and Jaoul (1996), Houlier et al. (1990), Jaoul et al. (1981, 1991), Grove et al. (1984), Yund (1986), Le Gall et al. (1994), Fielitz et al. (2007).

Ion diffusion properties in aluminosilicate melts inversely correlate with their viscosities, that is to say with their NBO/T (Hofmann, 1980; Shimizu and Kushiro, 1991; Mysen, 1988). The latter explicitly depends on the relative proportion of network formers and network destroyers, and hence the silica content is straightforwardly a first order parameter in determining NBO/T, viscosity and diffusivity. The lower is the NBO/T and the higher is the viscosity (Fig. 5). For example, the NBO/T is between 1 and 2 for

582 andesitic to mafic compositions (basalts), whilst it is < 0.1 for felsic compositions (rhyolites) and strictly
583 zero for dry silica. Consequently, the lower is the NBO/T and the lower is the diffusivity. An illustration
584 is given by Liang et al. (1996), who measured self–diffusivities in calcium aluminosilicate (CAS) melts
585 with low water contents between 0.04 – 0.07 wt.%. They show that D_{Si}, D_{Al}, D_O and D_{Ca} are respectively
586 about 20, 10, 13 and 4 times lower in the melt with 20, 15 and 65 wt.% CaO, Al_2O_3 and SiO_2 (NBO/T =
587 0.305) than with 40, 20, 40 wt. % CaO, Al_2O_3 and SiO_2 (NBO/T = 0.978).

588 In Figure 6 we present a compilation for diffusivities in silicates, considering: i) volume diffusion
589 in single crystals, ii) grain boundary diffusion in polycrystals, and iii) diffusion in melts. The considered
590 data were intentionally restricted to the slowest diffusing network formers (Al, Si and O), which are the
591 species susceptible to control the kinetics of diffusion controlled creep. To be in accord with the present
592 work, we further restricted our consideration to data obtained for dry systems. In the experimental
593 temperature range of interest the diffusion rates of Si and Al in silicate melts decrease over many orders
594 of magnitude with decreasing NBO/T, that is to say with increasing silica content and correspondingly
595 decreasing contents of network destroyers. In general, the diffusion rates are the fastest in basalts,
596 intermediate in rhyolitic melts and substantially lower in plagioclase melts. The extreme lowest diffusion
597 rate of Si in pure amorphous silica is nearly comparable with Si diffusion in single crystal pure quartz.
598 These observations are qualitatively consistent with our findings from creep data, which indicate: i) the
599 highest diffusivity for the partially molten samples of Dimanov et al. (2000), which contain amorphous
600 grain boundaries with ≈ 80 wt.% silica, ii) intermediate diffusivity for our SilLab1 samples, which present
601 amorphous grain boundaries with ≈ 85 wt.% silica, iii) the lowest diffusivity for our SilLab1 samples,
602 which present amorphous grain boundaries with ≈ 95 wt.% silica.

603 Yet, it is most important to address the question whether any silicate melt present along labradorite
604 grain boundaries may enhance the diffusion rates with respect to the crystalline grain boundaries. On the
605 one hand, the data of Dimanov et al. (2000) indicate that thin melt films with ≈ 80 wt. % silica provide

606 substantially faster pathways for grain boundary diffusion as compared with labradorite grain boundaries.
607 On the other hand, the present data for SilLab1 samples indicate that thin melt films with ≈ 85 wt.% silica
608 have no noticeable effect, whereas our data for SilLab5 samples indicate that grain boundary diffusion is
609 substantially slowed down within thin melt films with ≈ 95 wt.% silica. In order to be more quantitative
610 we need to estimate the effective diffusivities in our different samples and to compare the latter with
611 diffusivities in silicate melts and grain boundaries. For this purpose we considered the Eyring equation,
612 relating diffusivity and viscosity of liquids:
613
614 $$D_{eff} = \frac{k_B T}{\lambda \eta} \qquad (5)$$
615
616 where D_{eff} and η are respectively the effective diffusivity and the viscosity, and where the molecular radius
617 λ is taken as an approximation for the jump distance of the mobile species. For instance, the Eyring
618 equation is especially considered as applicable to the network formers in viscous silicate melts and glasses
619 (Mungal, 2002; Nascimento and Zanotto, 2006). Based on equation (5) and taking $\lambda = 10^{-10}$ m as a first
620 order approximation, we calculated the diffusivities of the melts present in SilLab1, SilLab5 and in the
621 partially molten labradorite (pmLab) of Dimanov et al. (2000). We show in Figure 6a that the latter are
622 intermediate between volume diffusion and grain boundary diffusion in silicates. Unfortunately, direct
623 measurements of grain boundary diffusivities for plagioclase materials are not available. Indirect
624 estimations of grain boundary diffusivities in plagioclase, pyroxene and forsterite from the kinetics of
625 reaction rim growth do exist (Liu et al., 1997; Yund, 1997; Yund and Farver, 1999; Milke et al., 2001;
626 Abart et al., 2004), but only for water present conditions, which precludes any direct comparison in the
627 present study. However, Figure 6b shows that the existing grain boundary diffusion data for dry silicates,
628 oxides and aluminosilicates (doted lines) correspond to the slowest diffusivities in the most polymerized
629 aluminosilicate melts (rhyolite, albite). This observation is in agreement with recent findings based on

molecular dynamics, which indicate strong similarities between the cooperative molecular motion at grain boundaries and in glass forming liquids (Zhang et al., 2009). According to the data, the calculated D_{eff} in labradorite partial melt (pmLab) corresponds very well to the measured Si and Al diffusivities in albite melt. On the other hand, we can highlight the fact that within the experimental range (1100 – 1300°C) D_{eff} in labradorite partial melt (pmLab) exceeds by about an order of magnitude the existing grain boundary diffusivities in enstatite, alumina and mulite. This observation is consistent with the findings of Dimanov et al. (2000), who reported that the partially molten laradorite samples (pmLab) were about an order of magnitude weaker than the fully crystalline samples. Conversely, the effective diffusion through melt films with 85 wt.% silica (SilLab1) seems slow enough to mimic grain boundary diffusion rates. This observation provides an explanation why the SilLab1 and the fully crystalline Lab samples have comparable strengths. Most interestingly, diffusion through melts with 95 wt. % silica (SilLab5) appears to be much slower than in any other melt, or at grain boundaries. The corresponding effective diffusivity is only one to two orders of magnitude faster than volume diffusion processes in aluminosilicate single crystals involving network formers (diffusion of Al and O in mullite and CaAl – NaSi interdiffusion in plagioclase). This observation clearly suggests very slow grain boundary diffusion rates for Sillab5 samples, which is fully consistent with the fact that the latter are considerably stronger than the SilLab1 and Lab samples.

4.3. Grain boundary diffusivity versus melt – grain interfacial diffusivity

We estimated on the basis of equations (4) and (5) the effective diffusivities for the different amorphous silicate materials present along grain boundaries in our partially molten plagioclase samples. The results are in good agreement with the extant diffusion data in dry conditions for Si, Al and O (network formers and rate liming species) in both aluminosilicate melts and along grain boundaries (Fig. 6). From

654 this comparison it appears that i) diffusivity in plagioclase – like partial melt (80 wt. % silica) is
655 substantially faster than diffusivities along grain boundaries; ii) diffusivities along grain boundaries
656 correspond to the diffusivity in silica – rich melt (85 wt. % SiO_2); iii) diffusivity in extremely silica – rich
657 melt (95 wt. % silica) is substantially slower than along grain boundaries. The first point indicates that
658 partially molten plagioclase containing plagioclase – like melt forming films along grain boundaries
659 should be weaker than nominally crystalline plagioclase, which is precisely what Dimanov et al. (2000)
660 observed. The second and the third points imply that partially molten plagioclase with silica – rich (85 wt.
661 % SiO_2) and extremely silica – rich (95 wt. % SiO_2) melt films along grain boundaries should be,
662 respectively, as strong- and stronger than nominally crystalline plagioclase, which is what we did observe.
663 Our evaluation of diffusivities from melt viscosities, which were previously evaluated from melt
664 chemistry, is only a first order approximation. Nevertheless, in spite of the roughness of this approach,
665 the order of magnitude and the consistency of the estimated results are convincingly reasonable when
666 compared with i) the experimental data for melts (Figures 5 and 6); ii) our creep data interpreted in terms
667 of efficiency of interfacial diffusion. However, these observations open some additional questions about
668 the structure and the diffusivities at the interfaces between the grains and the intergranular amorphous
669 films, which are developed below.

670 Solid state diffusional mass transfer operates owing to crystallographic structural defects. Volume
671 diffusion relies on point defects, such as vacancies, interstitials, substitution impurities and their
672 associations. Alternatives for faster volume diffusion are provided by extended linear and planar defects,
673 such as dislocation cores and twin boundaries or sub – grain boundaries. The latter are special low – angle
674 tilt – boundaries, which result from the rearrangement of free dislocations (dislocation pile-up) driven by
675 the associated decrease in free energy of the system. Twin boundaries and low – angle tilt – boundaries
676 may be called are coherent semi – coherent, respectively, because they present the most numerous
677 coincident crystallographic sites. Conversely, the common high angle, tilt and twist grain boundaries

present the lowest densities of coincident lattice sites. The lower is the density of the coincident lattice sites and inversely higher is the density of the structural defects (local lattice distortion, dangling bonds, impurity segregation...) of the considered interface. Interfacial diffusion is conditioned by the density of interfacial structural defects, and hence, diffusion along common grain boundaries is orders of magnitude faster than diffusion along coherent interfaces and volume diffusion. The classical hypothesis that diffusion creep is controlled by the slowest species diffusing through the fastest path ways implies in the case of nominally crystalline plagioclase creep control by the diffusion of network formers along grain boundaries. Conversely, the fastest path ways would be the interfacial melt films, if providing fastest diffusion kinetics than the crystalline interfaces. It may be, however, more difficult to identify the fastest path ways if the interfaces contain amorphous material where diffusion is supposedly slower than at crystalline high angle grain boundaries. If diffusion occurs through the melt films, the materiel would strengthen with respect to the nominally crystalline one, which is what we did observe. Still, a question remains whether faster diffusion could not proceed along the grain – melt interfaces, in which case the macroscopic behaviour would differ. In order to clarify this point it is necessary to compare the nature and the density of structural defects at a melt – grain interface with respect to a common grain boundary, which we attempt in the following.

Low – angle tilt – boundaries are low – energy (favoured) grain boundaries that present the highest densities of coincident lattice sites. From a geometrical viewpoint their cores have been recognized to form regular arrays of “structural units”, i.e. small atomic groups organized in a characteristic configuration (Sutton and Vitek, 1983). Conceptually, the “structural unit model” is equivalent to describe the interface as closely spaced lattice dislocations (sometimes called primary dislocations) whose elastic stress field concentrates closely to the core interface (Baluffi and Bristowe, 1984). As a consequence, such grain boundaries present little lattice distortion at long-range. More random interfaces (tilt and twist boundaries) were tentatively described by mixing different types of structural units corresponding to

different types of favoured boundaries (Sutton and Vitek, 1983), which was shown i) to be equivalent to the classical grain boundary dislocation (or secondary dislocation) structure (Baluffi and Bristowe, 1984), ii) to be of limited success (Sutton, 1989). Furthermore, considering such general interfaces Sutton and Baluffi (1987) concluded that a simple geometric framework cannot provide general rules for optimized (low energy) configurations, because the atomistic and bonding structures must be considered as well. Therefore, random interfaces necessarily exhibit the highest densities of structural misfits and correspondingly the high interfacial energies. The latter are actually partly compensated by local relaxation (rearrangement) of atomic positions at and near the core interface (Merkle, 1997). Relaxation results in various crystallographic distortions of the core boundary. The net result is a strong short range interfacial disordering, which makes the dynamic properties (mobility, co-operational transport and viscosity) of grain boundaries to mimic those of amorphous phases (Zhang et al., 2009). Therefore, the common (high – angle, twist and tilt) grain boundaries are characterized by the highest density of ionic/molecular crystal structural defects (impurities, vacancies, interstitials and their associations), but also extended crystal structural defects (dislocations, sub-grain boundaries, vacancy clusters...), which all contribute to the structural misfits, the so called "packing frustration" and the presence of unsatisfied dangling bonds. As the interfacial free energy relates to the density of the interfacial structural defects (van der Merwe, 2001), it increases gradually from twin – and low angle – to high angle boundaries, which exhibit the highest interfacial energies.

For ceramic materials (alumina, zirconia, SiC, Si_3N_4, $SrTiO_2$...) it has been demonstrated that thin (nm – sized) amorphous films may be thermodynamically stable at grain boundaries, because they may contribute to lower the interfacial free energy of the system (Clarke, 1987; Clarke et al., 1993; Wilkinson, 1993; Bobeth et al., 1999). In other words, an amorphous interphase may contribute to partly compensate for the inherent interfacial structural defects. For instance, in order to minimise the excess free energy associated with interfacial misfits the surrounding crystalline lattices can only modestly relax by limited

distortion. Conversely, a viscous amorphous phase could more efficiently accommodate to any interfacial structural misfit, providing molecular units to satisfy dangling bonds. The net result would be the reduction of interfacial lattice distortions and interfacial free energy, and thus, of the density of structural defects. If so, the diffusivities at the crystal – melt interface should be lowered with respect to the common grain boundary diffusivities as well. So finally, whether the presence of an interfacial amorphous phase would slow down or enhance the grain boundary diffusion rates would essentially depend on the diffusion properties through the amorphous material itself. In the present case, the extremely silica – rich amorphous phase present along grain boundaries of SilLab5 material tends to slows down the diffusion properties and the samples appear stronger.

5. Conclusions

We investigated high temperature (>1000°C) diffusion controlled creep of plagioclase aggregates containing limited amounts of partial melt (2 – 6 vol. %), with respect to the physical structure (crystalline / amorphous) of the grain boundaries. We specifically focused on the effect of melt chemistry in the situation of thin amorphous films (< 10 nm) wetting grain boundaries. For this purpose we applied sol – gel techniques and isostatic hot – pressing (300 MPa, T = 1150°C) in order to synthesize i) nominally crystalline plagioclase material (SilLab), ii) two types of partially molten plagioclase materials (SilLab1 and SilLab5), containing limited amounts of silica – rich partial melt, with contrasting chemistries. The SilLab nominally melt – free samples contained < 1 vol. % residual glass. The SilLab1 and SilLab5 partially molten plagioclase samples contained 2 and 6 vol. % of aluminosilicate melts with c.a. 85 wt. % and 95 wt. % $Si0_2$, respectively. The hot-pressed materials were fine grained (< 15 μm) and contained about 0.05 wt. % water species that could be dried out by annealing at 1100°C and at atmospheric pressure. Uniaxial compression creep tests were performed at temperatures and flow stresses between 1100 –

1250°C and 3 – 60 MPa, respectively. All samples showed dominantly linear viscous flow with a stress exponent n ~ 1 and nominally melt – free samples showed a grain size exponent m ~ – 3, indicating grain boundary diffusion control. Activation energies were 433 ± 14 kJ/mol, 520 ± 21 kJ/mol and 672 ± 18 kJ/mol for nominally melt – free samples, and for samples containing ~ 2 vol. % and 6 vol. % silica – rich melts, respectively. The samples containing ~ 6 vol. % melt presented the highest activation energy and were substantially stronger than all other samples. We explained the fact by the presence of the highly polymerized and viscous melt, with the highest silica content (~ 95 wt. % $Si0_2$), and thus, with the lowest diffusion rates.

Based on viscosity models for aluminosilicate melts (Giordano et al., 2006) we estimated the viscosities and the effective diffusivities of the melts present in our samples and in previously studied partially molten plagioclase samples (≈ 80 wt. % $Si0_2$, Dimanov et al., 2000). The data we obtain are in agreement while considering the extant diffusion data of network formers in silicate melts, with respect to their silica contents and polymerization states in dry conditions. Furthermore, we considered volume diffusion data in single crystals and grain boundary diffusivities in silicates and oxides polycrystals. Amorphous silica apart, volume diffusion data in single crystals are the lowest, whilst melt diffusivities are the highest. For the latter, the diffusivities inversely correlate with the polymerization degree. Grain boundary diffusion data are much higher than volume diffusion data, but they overlap with the diffusivities in highly polymerized aluminosilicate melts. Our findings indicate that grain boundary diffusivity in polycrystalline melt-free labradorite is i) comparable to those in highly polimerized silica-rich melts (~ 85 wt. % $Si0_2$), ii) considerably lower than those in labradorite partial melt (~ 80 wt. % $Si0_2$), iii) substantially higher than in extremely silica-rich melt (~ 95 wt. % $Si0_2$).

We demonstrated strong physical – chemical couplings between plagioclase rheology based on grain boundary diffusion controlled creep and the presence of aluminoisilicate melts. In the particular case where grain boundaries present amorphous structure the rheological properties are strongly related to the

774 melt chemistry, and more specifically to the silica content. The latter determines the polymerization
775 degree and hence the diffusion properties, depending on which samples may either weaken or strengthen.
776 Counter intuitively, our data show that the presence of thin amorphous films at grain boundaries may not
777 always ensure faster diffusion path ways. In turn, in dry conditions grain boundary transport properties
778 may be strongly hindered in the presence of melt films with extreme silica contents (> 90 – 95 wt. % $Si0_2$).
779

780 **Acknowledgements**

781

782 The author is grateful to Jianguo Huang and Michael Naumann who assisted with sample
783 preparation techniques and mechanical testing, to Richard Wirth for his help with TEM observations, to
784 Erik Rybacki for many stimulating discussions and to Georg Dresen, who kindly provided unlimited
785 access to his experimental facilities and unconditional support. The rheological and microstructural
786 investigation data are available.

787

788 **References**

789

790 Abart, R., Kunze, K., Milke, R., Sperb, R. and Heinrich, W., (2004), Silicon and oxygen self-diffusion in
791 enstatite polycrystals: the Milke et al. (2001) rim growth experiments revisited. Contrib. Mineral. Petrol.,
792 Vol. 147, 633-646.
793 Ashby, M.F. and Verall, R.A. (1973), Diffusion accomodated flow and superplasticity. Acta Metallurgica.
794 Vol. 21, 149-163.
795 Balluffi, R.W. and P.D. Bristowe (1984), On the structural unit/grain boundary dislocation model for grain
796 boundary structure. Surface Science, Vol. 144 (1), 28-43.

797 Baker, D.R., (1990), Chemical interdiffusion of dacite and rhyolite: anhydrous measurement at 1 atm and
798 at 10 kbar, application of transient state theory and diffusion in zoned magma chambers. Contrib. Mineral.
799 Petrol., Vol.104: 407-423.
800 Baker, D.R., (1992), Tracer diffusion of network formers and multicomponent diffusion in dacitic and
801 rhyolitic melts. Geochim. Cosmochim. Acta., Vol. 56, 462-473.
802 Baker, D.R., (1995), Diffusion of silicon and gallium (as an analogue for aluminum) network-forming
803 cations and their relationship to viscosity in albite melt. Geochim. Cosmochim. Acta., Vol. 59 (17), 3561-
804 3571.
805 Beeman M.L. and Kohlstedt, D.L. (1993), Deformation of Fine-Grained Aggregates of Olivine Plus Melt
806 at High Temperatures and Pressures. J. Geophys. Res., Vol. 98, B4, 6443-6452, doi:10.1029/92JB02697
807 Beere, W. (1975), The second stage of sintering of powder compacts. Acta Metal. 23(1), 139-145.
808 Béjina, F. and Jaoul, O., (1996), Silicon self-diffusion in quartz and diopside measured by nuclear micro-
809 analysis methods. Phys. Earth. Planet. Interiors, Vol. 97, 145-162.
810 Beran, A., (1986), A model of Water Allocation in Alkali Feldspar, Derived from Infrared-Specroscopic
811 Investigations. Phys. Chem. Minerals, Vol. 13, 306-310.
812 Beran, A., (1987), O.H. Groups in Nominally Anhydrous Framework Structures: An Infrared
813 Spectroscopic Investigation of Danburite and Labradorite. Phys. Chem. Minerals, Vol.14, 441-445.
814 Brebec, G., Seguin, R., Sella, C., Benevot, J. and Martin, J.C., (1980), Diffusion du silicium dans la silice
815 amorphe. Acta Metall., Vol. 28, 327-333.
816 Bobeth, M., Clarke, D.R. and Pompe, W. (1999), A diffuse interface description of intergranular films in
817 polycrystalline ceramics. J. Am. Ceram. Soc., Vol. 82 (6), 1537-1546.
818 Bulau, J.R., Waff, H.S. and Tyburczy, J., (1979), Mechanical and thermodynamic constraints on fluid
819 distribution in partial melts. J. Geophys. Res., vol. 84, B11, 6102-6108.

820 Burger, P., Duclos, R. and Crampon, J., (1995), Microstructure characterization in superplastically
821 deformed silicon nitride. J. Am. Ceram. Soc., Vol. 80, 879-885.
822 Bussod, G.Y and Christie J.M. (1991), Textural development and melt topology in spinel lherzolite
823 experimentally deformed at hypersolidus conditions. J. Petrol. Special lherzolite issue, 17–39.
824 Bystricky, M., and S. Mackwell (2001), Creep of dry clinopyroxene aggregates, J. Geophys. Res., Vol.
825 106, 13443-13454.
826 Canil, D. and Muehlenbachs, K., (1990), Oxygen diffusion in an Fe-rich basalt melt. Geochim.
827 Cosmochim. Acta., Vol. 54: 2947-2951.
828 Carapic, G., Faul, U.H. and Brisson, E. (2013), High-resolution imaging of the melt distribution in
829 partially molten upper mantle rocks: evidence for wetted two-grain boundaries. Geochem. Geophys.
830 Geosyst., Vol. 14(3), 556-566 doi:10.1029/2012GC004547.
831 Chakraborty, S., Dingwell, D.B. and Rubie, D.C., (1995), Multicomponent diffusion in ternary silicate
832 melts in the system K_2O-Al_2O_3-SiO_2: II. Mechanisms, systematics, and geological implications.
833 Geochim. Cosmochim. Acta., Vol. 59(2), 265-277.
834 Clarisse L., Petit F., Crampon J. and Duclos R., (2000), Characterization of grain boundary sliding in a
835 fine-grained alumina-zirconia ceramic composite by atomic force microscopy. Ceram. Int., Vol. 26(3),
836 295-302.
837 Clarke, D.R., (1987), On the equilibrium thickness of intergranular glass phases in ceramic materials. J.
838 Am. Ceram. Soc., Vol. 70, 15-22.
839 Clarke D.R., Shaw, T.M., Philipse, A.P. and Horn, R.G. (1993), Possible electrical double layer
840 contribution to the equilibrium thickness of intergranular glass films in polycrystalline ceramics. J. Am.
841 Ceram. Soc., Vol. 76(5), 1201-1204.
842 Cmíral, M., Fitz Gerald, J.D., and Faul, U.H., (1998), A close look at dihedral angles and melt geometry
843 in olivine-basalt aggregates: a ZEM study, Contib Minearal Petrol, Vol.130, 336-345.

844 Coble, R.L., (1963), A model for boundary diffusion controlled creep in polycrystalline materials. J. Appl.
845 Phys., Vol. 34, 1679-1682.
846 Cooper, R.F. and Kohlstedt, D.L., (1984a), Sintering of olivine and olivine – basalt aggregates. Phys.
847 Chem. Mineral., Vol. 11, 5 – 6.
848 Cooper, R.F. and Kohlstedt, D.L., (1984b), Solution - precipitation enhanced diffusional creep of partially
849 molten olivine-basalt aggregates during hot-pressing. Tectonophysics, Vol. 107, 207-233.
850 Cooper, R.F. and Kohlstedt, D.L., 1986. Rheology and Structure of Olivine - Basalt Partial Melts. J.
851 Geophys. Res. Vol. 91, B9, 9315-9323.
852 Cooper, R.F., Kohlstedt, D.L. and Chyung. K., (1989), Solution-precipitation enhanced creep in solid-
853 liquid aggregates which display a non-zero dihedral angle. Acta Metall., Vol. 37, 1759-1771.
854 Daines, M.J. and Kohlstedt, D.L., (1997), Influence of deformation on melt topology in peridotites. J.
855 Geophys. Res., Vol. 102, B5, 10257-10271.
856 Dell'Angelo, L.N. and Tullis, J., (1988), Experimental deformation of partially melted granitic aggregates.
857 J. Metamorph. Geol., Vol. 6, 495-515.
858 Dell'Angelo, L.N., Tullis, J. and Yund, R.A., (1987), Transition from dislocation creep to melt-enhanced
859 diffusion creep in fine grained granitic aggregates. Tectonophysics, Vol. 139, 325-332.
860 Dimanov, A., Dresen, G. and Wirth, R., (1998), High-temperature creep of partially molten plagioclase
861 aggregates. J. Geophys. Res., Vol. 103, B5, 9651-9664.
862 Dimanov, A., Xiao, X., Dresen G. and Wirth. R., (1999), Grain Boundary Diffusion Creep of Synthetic
863 Anorthite: The Effect of Water. J. Geophys. Res., Vol. 104, 10483-10497.
864 Dimanov, A., Wirth, R. and Dresen, G., (2000), The effect of melt distribution on the rheology of feldspar
865 rocks. Tectonophysics, Vol. 328, 307-327.
866 Dimanov, A., Lavie, M.P., Ingrin, J., Dresen, G. and Jaoul, O. (2003), Creep of polycrystalline anorthite
867 and diopside. J. Geophys. Res. Vol. 108, B1, 2061, doi:10.10292002JB001815.

868 Dimanov, A., Rybacki, E., Wirth, R. and Dresen G. (2007), Creep and strain-dependent microstructures
869 of synthetic anorthite-diopside aggregates: J. Struct. Geol., Vol. 29, 1049–1069, doi:
870 10.1016/j.jsg.2007.02.010.
871 Dimanov, A., Raphanel, J. and Dresen G. (2011), Newtonian flow of heterogeneous synthetic gabbros at
872 high strain: Grain sliding, ductile failure, and contrasting local mechanisms and interactions. Eur. J. Min.,
873 Vol. 23(3), 303-322, doi: 10.1127/0935−1221/2011/0023−2110
874 Dimanov A. and Dresen, G. (2005), Rheology of synthetic anorthite-diopside aggregates: Implications
875 for ductile shear zones. J. Geophys. Res., Vol. 110, doi:10.1029/2004JB003431.
876 De Kloe, R., Drury, M.R., and van Roermund, H.L.M., (2000), Evidence for stable grain boundary melt
877 films in experimentally deformed olivine –orthopyroxene rocks, Phys Chem Minerals, Vol. 27, 480-494.
878 Drury, M.R. and FitzGerald, J.D., (1996), Grain boundary melt films in an experimentally deformed
879 olivine-orthopyroxene rock: implications for melt distribution in upper mantle rocks. Geophys. Res. Lett.,
880 Vol. 23(7), 701-704.
881 Duclos, R., Crampon, J. and Carry, C., (2002), Grain-boundary sliding and accommodation mechanism
882 during creep of yttria-partially-stabilized zirconia. Philos. Mag. Lett., Vol. 82(10), 529-533.
883 Faul, U.H., (1997) Permeability of partially molten upper mantle rocks from experiment and percolation
884 theory. J. Geophys. Res., Vol. 102, B5, 10299-10311.
885 Fielitz, P., G. Borchardt, M. Schmüker, H. Schneider and P. Willich (2004), Oxygen grain-boundary
886 diffusion in polycrystalline Mullite Ceramics. J. Am. Ceram. Soc., Vol. 87(12), 2232-2236. doi:
887 10.1111/j.1151-2916.2004.tb07497.x
888 Fielitz, P., G. Borchardt, M. Schmüker and H. Schneider (2007), A diffusion-controlled mullite formation
889 reaction model based on tracer diffusivity data for aluminium, silicon and oxygen. Phil. Mag., Vol. 87(1),
890 111-127.

Fielitz,P. and G. Borchardt (2016), Self-Diffusion of the Constituent Elements in Alpha-Alumina, Mullite and Aluminosilicate Glasses", Diffusion Foundations, Vol. 8, 80-108.

Nascimento, M.L.F. and E.D. Zannoto, (2006), Mechanisms and dynamics of crystal growth, viscous flow, and self-diffusion in silica glass. Phys. Rev. B, Vol. 73, 024209.

Fisler, D.K. and Mackwell, S.J., (1994), Kinetics of diffusion-controlled growth of fayalite. Phys. Chem. Minerals, Vol. 21, 156-165.

Fisler, D.K., Mackwell, S.J. and Petsch, S., (1997), Grain boundary diffusion in enstatite. Phys. Chem. Minerals, Vol. 24, 264-273.

Franz, L. and Wirth, R., (1997), Thin intergranular melt films and melt pockets in spinel peridotite xenoliths from the Rhön area (Germany): early stage of melt generation by grain boundary melting. Contrib. Mineral. Petrol., Vol. 129 (4), 268-283.

Fujii, N., K. Osamura and E. Takahashi (1986), Effect of water saturation on the distribution of partial melt in the olivine-pyroxene-plagioclase system. J. Geophys. Res., Vol. 91, 9253-9259.

Giordano, D. and Dingwell, D.B. (2003), Non-Arrhenian multicomponent melt viscosity: A model. Earth Planet. Sci. Lett., Vol. 208, 337–349.

Giordano, D., Mangicapra, A., Potuzak, M., Russell, J.K., Romano, C., Dingwell, D.B. and Di Muro, A. (2006), An expanded non-Arrhenian model for silicate melt viscosity: A treatment for metaluminous, peraluminous and peralkaline melts. Chem. Geol., Vol. 229, 42–56.

Giordano, D., Russell, J.K. and Dingwell, D.B. (2008), Viscosity of magmatic liquids: a model. Earth and Planet. Sci. Letts., Vol. 271, 123-134.

Grove, T.L., Baker, M.B. and Kinzler, R.J., (1984), Coupled CaAl - NaSi diffusion in plagioclase feldspar: experiments and applications to cooling rate speedometry. Geochim. Cosmochim. Acta., Vol. 48, 2113-2121.

914 Hamilton, D.L., and Henderson, C.M.B. (1968), The preparation of silicate compositions by a gelling
915 method. Mineral. Mag., Vol. 36, 832-838.
916 Harmer M.P. and Brook R.J., (1980), The effect of MgO additions on the kinetics of hot pressing in
917 Al_2O_3. J. Mater. Sci., Vol. 15, 3017-3024.
918 Harris, N. (2007), Channel flow and the Himalayan–Tibetan orogen: a critical review, J. Geol. Soc., Vol.
919 164(3), 511-523, doi: 10.1144/0016-76492006-133
920 Hess, P.C., (1994), Thermodynamics of thin fluid films. J. Geophys. Res., Vol. 99, B4, 7219-7229.
921 Hetherington, G., Jack, K.H. and Kennedy, J.C. (1964), The viscosity of vitreous silica. Phys. Chem.
922 Glass., Vol. 5, 130-136.
923 Hier-Majumder, S., P.H. Leo and D.L. Kohlstedt (2004), On grain boundary wetting during deformation.
924 Acta Mater. Vol. 52, 3425-3433, doi:10.1016/j.actamat.2004.03.040
925 Hier-Majumder, S., S. Mei, and D.L. Kohlstedt (2005), Water weakening of clinopyroxene in the diffusion
926 creep regime, J. Geophys. Res. Vol. 110, B07406, doi:10.1029/2004JB003414
927 Hiraga, T., Anderson, I., Zimmerman, M., Mei, S. and Kohlstedt, D. (2002), Structure and chemistry of
928 grain boundaries in deformed, olivine + basalt and partially molten lherzolite aggregates: evidence of
929 melt-free grain boundaries. Contrib. Mineral. Petrol., Vol. 144, 163-175, doi: 10.1007/s00410-002-0394-
930 1
931 Hirth, G. and Kohlstedt, D.L., (1995a), Experimental constraints on the dynamics of the partially molten
932 upper mantle: Deformation in the diffusion creep regime. J. Geophys. Res., Vol. 100, B2, 1981-2001.
933 Hirth, G. and Kohlstedt, D.L., (1995b), Experimental constraints on the dynamics of the partially molten
934 upper mantle: 2 Deformation in the dislocation creep regime. J. Geophys. Res. Vol. 100, B8, 15441-
935 15449.
936 Hofmann, A.W. (1980), Diffusion in silicate melts: a critical review. In Physics of Magmatic Processes
937 (ed. R.B. Hargraves), 385-417. Princeton Univ. Press.

938 Hofmeister, A. and Rossman, G., (1985), A model for the Irradiative Coloration of Smoky Feldspar and
939 the Inhibiting Influence of Water. Phys. Chem. Mineral., Vol. 12: 324-332.
940 Holtzman, B., Groebner, N., Zimmerman, M., Ginsberg, S. and Kohlstedt, D. (2003), Stress-driven melt
941 segregation in partially molten rocks. Geochem. Geophys. Geosyst., Vol. 4, Art. No. 8607.
942 Holtzman B.K. and Kohlstedt D.L., (2007), Stress driven melt segregation and strain partitioning in
943 partially molten rocks: Effects of stress and strain. J. Petrol., Vol. 48, 2379-2406.
944 Houlier, B., Cheraghmakani, M., Jaoul, O., (1990), Silicon diffusion in San-Carlos olivine. Phys. Earth
945 Planet. Interiors., Vol. 62, 329-340.
946 Huang, Y. and Langdon, T.G. (2002), Characterization of deformation processes in a Zn-22% Al alloy
947 using atomic force microscopy. J. Mat. Sci., Vol. 37(23), 4993-4998.
948 Ildefonse, B. and Nicolas, B. (1997), Ecoulement magmatique dans les gabbros et problème des chambres
949 magmatiques sous les dorsales océaniques. In "Des grands écoulements naturels à la dynamique du tas de
950 sable : introduction aux suspensions concentrées en géologie et en physique" (B. Ildefonse, C. Allain &
951 P. Coussot, eds.), Cemagref Editions, 37-49.
952 Jaoul, O., Poumellec, M., Froidevaux, A. and Havette, A., (1981), Silicon diffusion in forsterite: a new
953 constraint for understanding mantle deformation. In Anelasticity in the Earth (Stacey FD, Paterson MS
954 and Nicolas A Eds.), AGU Geodyn. Ser. Vol. 4, 95-100.
955 Jaoul, O., Sautter, V. and Abel, F. (1991), Nuclear microanalysis: A powerful tool for measuring low
956 atomic diffusivity with mineralogical applications. In "Advances in Physical Geochemistry, Diffusion,
957 Atomic Ordering, and Mass Transport: Selected Problems in Geochemistry", J. Ganguly, ed., Springer-
958 Verlag, Berlin, Vol. 6, 198-200.
959 Jin, Q., Wilkinson, D.S. and Weatherly, G.C. (1995), Redistribution of a grain boundary glass phase
960 during creep of Si_3N_4 ceramics. J. Am. Ceram. Soc., Vol. 72: 211-214.

961 Jin, Z.M., Green, H.W. and Zhou, Y. (1994), Melt topology in partially molten mantle peridotite during
962 ductile deformation. Nature, Vol. 372, 164-167.
963 Jung, H. and Waff, H.S. (1998), Olivine crystallographic control and anisotropic melt distribution in
964 ultramafic partial melts. Geophys. Res. Lett., Vol. 25, 2901-2904.
965 Jurewitz, S. R. and E. B. Watson (1985), The distribution of partial melt in a granitic system: the
966 application of liquid phase sintering theory. geochim. Cosmochim. Acta, Vol. 49, 1109-1121.
967 Kajihara, K., Yoshizawa, Y. and Sakuma, T. (1995), The enhancement of superplastic flow in tetragonal
968 zirconia polycrystals with SiO_2-doping. Acta Metall. Mater. Vol. 43, 1235-1242.
969 Katz R.F., Spiegelman M. and Holtzman B. (2006), The dynamics of melt and shear localization in
970 partially molten aggregates, Nature, Vol. 442, 676-679.
971 Kohlstedt, D.L. (1992), Structure, Rheology and permeability of partially Molten Rocks at Low Melt
972 Fractions. Mantle Flow and Melt Generation at Mid - Ocean Ridges. AGU Geophys. Monograph Vol. 71,
973 10-121.
974 Kohlstedt, D.L. and Zimmermann, M.E. (1996), Rheology of partially molten mantle rocks. Annu. Rev.
975 Earth Planet. Sci., Vol. 24, 41-62.
976 Kress, V.C. and Ghiorso, M.S. (1995), Multicomponent diffusion in basaltic melts. Geochim.
977 Cosmochim. Acta. Vol. 59(2) 313-324.
978 Lamoureux, G., B. Ildefonse, and D. Mainprice (1999), Modelling the seismic properties of fast-spreading
979 ridge crustal LVZ: insights from Oman gabbro textures. Tectonophysics, Vol. 312, 283–301.
980 Laporte, D. and Watson, E.B. (1995), Experimental and theoretical constraints on melt distribution in
981 crustal sources: the effect of crystalline anisotropy on melt interconnectivity. Chem. Geol., Vol. 124, 161-
982 184.

983 Laporte, D., Rapaille, C. and Provost, A. (1997), Wetting angles, equilibrium melt geometry, and the
984 permeability threshold of partially molten crustal protoliths. In Granite: from segregation of melt to
985 emplacement fabrics. (ed. J.L. Bouchez), Kluwer Academic Publishers, Netherlands, 31-54.
986 Legall, M., Lesage, B. and Bernardini, J. (1994), Self-diffusion in alpha-Al2O3. 1. Aluminium diffusion
987 in single-crystals. Philos. Mag. A, Vol. 70(5), 761-773.
988 Lesher, C.E., Hervig, R.L. and Tinker, D. (1996), Self diffusion of network formers (silicon and oxygen)
989 in naturally occuring basaltic liquid. Geochim. Cosmochim. Acta. Vol. 60(3), 405-413.
990 Liang, Y., Richter, F.M., Davis, A.M. and Watson, B. (1996), Diffusion in silicate melts: I. Self-diffusion
991 in CaO – Al2O3 – SiO2 at 1500°C and 1 GPa. Geochim. Cosmochim. Acta., Vol. 60, 4353-4367.
992 Liu, M., Peterson, J.C. and Yund, R.A. (1997), Diffusion-controlled growth of albite and pyroxene
993 reaction rims. Contrib. Mineral. Petrol., Vol. 126, 217-223.
994 Mecklenburgh, J. and Rutter, E.H. (2003), On the rheology of partially molten synthetic granite. J. Struct.
995 Geol., Vol. 25, 1575-1585.
996 Meléndez-Martinez, J.J. and Dominguez-Rodriguez, A. (2004), Creep of silicon nitride. Prog. Mat. Sci.,
997 Vol. 49, 19-107.
998 Mei, S. and Kohlstedt, D.L. (2000), Influence of Water on Plastic Deformation of Olivine Aggregates: 1.
999 Diffusion Creep Regime. J. Geophys. Res. Vol. 105(21), 457-21,469.
1000 Mei, S., Bai, W., Hiraga, T. and Kohlstedt, D.L. (2002), Influence of melt on the creep behaviour of
1001 olivine – basalt aggregates under hydrous conditions. Earth Planet. Sci. Lett. Vol. 201, 491 – 507.
1002 Merkle, K.L., (1997), Atomic-Scale Grain Boundary Relaxation Modes in Metals and Ceramics.
1003 Microscopy and Microanalysis, Vol. 3(4), 339-351.
1004 Milke, R., Wiedenbeck, M. & Heinrich, W. (2001), Grain boundary diffusion of Si, Mg, and O in enstatite
1005 reaction rims: a SIMS study with isotopically doped reactands. Contrib Mineral Petrol, Vol. 14, 15-26.
1006 Mysen B.O. (1983), The structure of silicate melts, Ann. Rev. Earth Planet Sci., Vol. 11, 75-97.

1007 Mysen, B.O. (1988), Structure and Properties of Silicate Melts. Elsevier, pp 354.

1008 Mysen, B.O. (2003), Physics and chemistry of silicate glasses and melts. Eur. J. Mineral. Vol. 15, 781-
1009 802.

1010 Mungal, J.E. (2002), Empirical models relating viscosity and tracer diffusion in magmatic silicate melts.
1011 Geochim. Cosmochim. Acta., Vol. 66 (1), 125-143.

1012 Nascimento, M.L.F. and Zanotto, E.D. (2006), Mechanisms and dynamics of crystal growth, viscous flow
1013 and self-diffusion in silica glass. Phys. Rev. B, Vol. 73, 024209.

1014 Nicolas, A. and Ildefonse, B. (1996), Flow mechanism and viscosity in basaltic magma chambers.
1015 Geophys. Res. Lett., Vol. 16, 2013-2016.

1016 Ojovan, M.I. and Lee W.E., (2004), Viscosity of network liquids within Doremus approach. J. Appl. Phys.
1017 Vol. 95, 3803-3810.

1018 Paterson, M.S., (1982), The determination of hydroxyl by infrared absorption in quartz, silicate glass and
1019 similar materials. Bull. Mineral., Vol. 105, 20-29.

1020 Paterson, M.S. (2001), A granular flow theory for the deformation of partially molten rock.
1021 Tectonophysics, Vol. 335, 51-61.

1022 Pharr, G.M. and Ashby, M.F. (1983), On creep enhanced by a liquid phase. Acta Metall., Vol. 31, 129-
1023 138.

1024 Raj, R. (1982), Creep in polycrystalline aggregates by matter transport through a liquid phase. J. Geophys.
1025 Res. Vol. 87, B6, 4731-4739.

1026 Rubie D.C. (1986), The catalysis of mineral reactions by water and restrictions on the presence of aqueous
1027 fluid during metamorphism. Mineral. Mag., Vol. 50, 399-415.

1028 Russell, J.K. and Giordano, D. (2005), A model for silicate melt viscosity in the System CaMgSi2O6–
1029 CaAl2Si2O8–NaAlSi3O8. Geochim. Cosmochim. Acta Vol. 69, 5333-5349.

1030 Giordano, D., J. K. Russell and D.B. Dingwell (2008), Viscosity of magmatic liquids: A model, Earth and
1031 Planet Sci Lett, Vol. 271, 123-134.
1032 Reid, J.E., B.T. Poe, D.C. Rubie, N. Zotov, M. Wiedenbeck (2001), The self-diffusion of silicon and
1033 oxygen in diopside ($CaMgSi_2O_6$) liquid up to 15 GPa. Chem. Geol., Vol. 174, 77–86.
1034 Rybacki, E. and Dresen, G. (2000), Dislocation and diffusion creep of synthetic anorthite aggregates. J.
1035 Geophys. Res., Vol. 105 (B11), 26017-26036. DOI:10.1029/2000JB900223
1036 Schäfer, F.N. and Foley, S.F. (2002), The effect of crystal orientation on the wetting behaviour of silicate
1037 melts on the surfaces of spinel peridotite minerals. Contrib. Meneral. Petrol., Vol. 143(2), 254-262.
1038 Shimizu, N. and Kushiro, I. (1984), Diffusivity of oxygen in jadeite and diopside melts at high pressures.
1039 Geochim. Cosmochim. Acta., Vol. 48, 1295-1303.
1040 Shimizu, N. and Kushiro, I. (1991) The mobility of Mg, Ca and Si in diopside-jadeite liquids at high
1041 pressures. In Physical Chemistry of Magmas, Advances in Physical Geochemistry, (eds. L.L. Perchuk and
1042 I. Kushiro), Vol. 9, 192-212, Springer-Verlag.
1043 Spiess, R., Dibona, R., Rybacki, E., Wirth, R. and Dresen, G. (2012), Depressurized Cavities within High-
1044 strain Shear Zones: their Role in the Segregation and Flow of SiO2-rich Melt in Feldspar-dominated
1045 Rocks. J. Petrol., Vol. 53(9), 1767-1776. doi:10.1093/petrology/egs032.
1046 Sutton, A.P. and V. Vitek (1983), On the Structure of Tilt Grain Boundaries in Cubic Metals I.
1047 Symmetrical Tilt Boundaries. Phil. Trans. Roy. Soc. London A, Vol. 309, 1-36;
1048 DOI:10.1098/rsta.1983.0020.
1049 Sutton, A.P. and Baluffi R.W. (1987), Overview no. 61 On geometric criteria for low interfacial energy.
1050 Acta Metall. Vol. 35 (9), 2177-2201.
1051 Sutton, A.P. (1989), On the structural unit model of grain boundary structure. Phil. Mag. Lett. Vol. 59 (2),
1052 53-59.

1053 Urbain, G. Y. Bottinga and P. Richet (1982), Viscosity of liquid silica, silicates and alumino-silicates.
1054 Geochim. Cosmochim. Acta, Vol. 46 (6), 1061–1072.
1055 Van der Molen, I. and Paterson, M.S. (1979), Experimental deformation of partially molten granite.
1056 Contrib. Mineral. Petrol., Vol. 70, 299-318.
1057 van der Merwe (2001), Interfacial energy: bicrystals of semi-infitite crystals. Prog. Surf. Sci., Vol. 67,
1058 356-381.
1059 Vigneresse, J.L., Barbey, P. and Cuney, M. (1996), Rheological transitions during partial melting and
1060 crystallization with application to felsic magma sgregation and transfer. J. Petr., Vol. 37, 1579-1600.
1061 Von Bargen, N. and Waff, H.S. (1986), Permeabilities, interfacial areas and curvatures of partially molten
1062 systems: Results of numerical computations of equilibrium microstructures. J. Geophys. Res., Vol. 91,
1063 B9, 9261-9276.
1064 Waff, H.S. and Bulau J.R. (1979), Equilibrium fluid distribution in an ultramafic partial melt under
1065 hydrostatic stress conditions. J Geophys Res., Vol. 84, 6109–6114.
1066 Waff, H.S. and J.R. Bulau (1982), Experimental studies of near-equilibrium textures in partially molten
1067 silicates at high pressures. In High Pressure Res. Geophys., Adv. Earth Planet. Sci., Vol. 12, 229-236.
1068 Waff, H.S. and Faul, U.H. (1992), Effects of crystalline anisotropy on fluid distribution in ultramafic
1069 partial melts. J. Geophys. Res., Vol. 97, 9003-9014.
1070 Walte, N.P., P.D. Bons, C.W. Passchier and D. Koehn (2003), Disequilibrium melt distribution during
1071 static recrystallization. Geology, Vol. 31, 1009–1012.
1072 Wanamaker, B.J. and Kohlstedt, D.L. (1991), The effect of melt composition on the wetting angle between
1073 silicate melts and olivine. Phys. Chem. Mineral., Vol. 18, 26-36.
1074 Wolfenstine, J. and Kohlstedt, D.L. (1994), High-temperature creep and kinetic decomposition of
1075 Ni_2SiO_4. Phys. Chem. Mineral., Vol. 21, 234-243.

1076 Wang, Z., Dresen, G. and Wirth, R. (1996), Diffusion creep of fine-grained polycrystalline anorthite at
1077 high temperature, Geophysical Research Letters, Vol. 23, 3111-3114.
1078 Wark, D.A., Williams, C.A., Watson, E.B., Price, J.D. (2003), Reassessment of pore shapes in
1079 microstructurally equilibrated rocks, with implications for permeability of the upper mantle. J. Geophys.
1080 Res. Vol. 108 (B1), 2050. doi:10.1029/ 2001JB001575
1081 Wendlandt, R.F. (1991), Oxygen diffusion in basalt and andesite melts: experimental results and
1082 discussions of chemical versus tracer diffusion. Contrib. Mineral. Petrol. Vol. 108, 463-471.
1083 Wilkinson, D.S. (1998), Creep Mechanisms in Multi-phase Ceramic Materials, Feature Article, J. Amer.
1084 Ceram. Soc., Vol. 81, 275-299.
1085 Wirth, R. (1996), Thin amorphous films (1-2 nm) at olivine grain boundaries in mantle xenoliths from
1086 San Carlos, Arizona. Contrib. Mineral. Petrol., Vol. 124, 44-54.
1087 Yund, R.A. (1986), Interdiffusion of NaSi-CaAl in Peristerite. Phys. Chem. Minerals, Vol. 13, 11-16.
1088 Yund, R.A. (1997), Rates of grain boundary diffusion through enstatite and forsterite reaction rims.
1089 Contrib. Mineral. Petrol., Vol. 126, 224-236.
1090 Yund, R.A. and Farver, J.R. (1999), Si grain boundary diffusion rates in feldspar aggregates. Abstr. EOS,
1091 supl. F1077.
1092 Zhang, H., Srolovitz, D.J., Douglas, J. F. and Warren, J.A. (2009), Grain boundaries exhibit the dynamics
1093 of glass-forming liquids, Proc. Nat. Acc. Sci., Vol. 106(19), 7735–774.
1094 Zimmerman, M.E. and Kohlstedt, D.L. (1999), Influence of deformation mechanism on melt topology in
1095 partially molten peridotites. EOS Trans. AGU Suppl., 80, S326.
1096 Zimmerman, M., Zhang, E., Kohlstedt, D. and Karato, S. (1999), Melt distribution in mantle rocks
1097 deformed in shear. Geophys. Res. Letts., Vol. 26, 1505-1508.